NORSAR

Scientific Report No. 2 - 81/82

SEMIANNUAL TECHNICAL SUMMARY

1 October 1981—31 March 1982

By
Jørgen Torstveit (ed.)

Kjeller, July 1982

SECURITY CLASSIFICATION OF THIS PAGE *(When Data Entered)*

REPORT DOCUMENTATION PAGE		READ INSTRUCTIONS BEFORE COMPLETING FORM
1. REPORT NUMBER F08606-79-C-0001	2. GOVT ACCESSION NO.	3. RECIPIENT'S CATALOG NUMBER
4. TITLE *(and Subtitle)* SEMIANNUAL TECHNICAL SUMMARY 1 October 1981 - 31 March 1982		5. TYPE OF REPORT & PERIOD COVERED 1 Oct 81 - 31 Mar 82
		6. PERFORMING ORG. REPORT NUMBER Sci. Report 2/81-82
7. AUTHOR(s) J. Torstveit (ed.)		8. CONTRACT OR GRANT NUMBER(s)
9. PERFORMING ORGANIZATION NAME AND ADDRESS NTNF/NORSAR Post Box 51 N-2007 Kjeller, Norway		10. PROGRAM ELEMENT, PROJECT, TASK AREA & WORK UNIT NUMBERS NORSAR Phase 3
11. CONTROLLING OFFICE NAME AND ADDRESS AFTAC/HQ/TGX Patrick AFB FL 32925		12. REPORT DATE July 1982
		13. NUMBER OF PAGES 73
14. MONITORING AGENCY NAME & ADDRESS(if different from Controlling Office) USA		15. SECURITY CLASS. (of this report)
		15a. DECLASSIFICATION/DOWNGRADING SCHEDULE

16. DISTRIBUTION STATEMENT *(of this Report)*

APPROVED FOR PUBLIC RELEASE; DISTRIBUTION UNLIMITED.

17. DISTRIBUTION STATEMENT *(of the abstract entered in Block 20, if different from Report)*

18. SUPPLEMENTARY NOTES

19. KEY WORDS *(Continue on reverse side if necessary and identify by block number)*

20. ABSTRACT *(Continue on reverse side if necessary and identify by block number)*

This report describes the operation, maintenance and research activities at the Norwegian Seismic Array (NORSAR) for the period 1 October 1981 to 31 March 1982.

DD FORM 1 JAN 73 **1473**   EDITION OF 1 NOV 65 IS OBSOLETE

The uptime of the NORSAR online detection processor system has averaged 91.9%, which represents an improvement of 3% compared to the previous period. Almost half of the downtime was due to problems in connection with the termination of the NORSAR ARPANET circuit. The SPS has been working well and has caused less than 1% downtime.

A total of 1681 events were reported in this period, giving a daily average of 9.2 events. The number of reported events per month varies from 210 in February to 363 in December.

There have been no major breakdowns on the communications lines, but some lines have had periods with bad performance, especially the 02C line.

The new DP system to be implemented on IBM 4331/MODCOMP is now, except for some EOC functions, ready. The communication problem between IBM 4331 and Modcomp has been solved, and test runs have been done with no errors. Some improvements in programs and some more testing still needs to be done before the new DP is ready to replace the current system.

The research activity is briefly described in Section VI. The subsection 1 discusses a method for simultaneous determination of source parameters. Subsection 2 presents a processing package for on-line analysis of data from small-aperture arrays. Subsection 3 is a study on optimization of seismic array configuration. Subsection 4 and 5 describe the upper mantle seismic heterogeneities beneath Fennoscandia and Eastern Europe. Subsection 6 describes a work for mapping the crustal structure and thickness in the coastal areas of southern Norway and the general features of the Moho near and in the Oslo Graben. Subsection 8 is a noise study at various sites in Finland, in northern Norway and in southeastern Norway.

AFTAC Project Authorization No.	:	VELA VT/0702/B/PMP, Amendment 1
ARPA Order No.	:	2551
Program Code No.	:	0F10
Name of Contractor	:	Royal Norwegian Council for Scientific and Industrial Research
Effective Date of Contract	:	1 October 1979
Contract Expiration Date	:	30 September 1982
Project Manager	:	Frode Ringdal (02) 71 69 15
Title of Work	:	The Norwegian Seismic Array (NORSAR) Phase 3
Amount of Contract	:	$3.500.000
Contract Period Covered by the Report	:	1 October 1981 – 31 March 1982

TABLE OF CONTENTS

TABLE OF CONTENTS (cont.)

I.   SUMMARY

This report describes the operation, maintenance and research activities at the Norwegian Seismic Array (NORSAR) for the period 1 October 1981 to 31 March 1982.

The uptime of the NORSAR online detection processor system has averaged 91.9%, which represents an improvement of 3% compared to the previous period. Almost half of the downtime was due to problems in connection with the termination of the NORSAR ARPANET circuit. The SPS has been working well and has caused less than 1% downtime.

A total of 1681 events were reported in this period, giving a daily average of 9.2 events. The number of reported events per month varies from 210 in February to 363 in December.

There have been no major breakdowns on the communications lines, but some lines have had periods with bad performance, especially the 02C line.

The new DP system to be implemented on IBM 4331/MODCOMP is now, except for some EOC functions, ready. The communication problem between IBM 4331 and Modcomp has been solved, and test runs have been done with no errors. Some improvements in programs and some more testing still needs to be done before the new DP is ready to replace the current system.

The research activity is briefly described in Section VI. The subsection 1 discusses a method for simultaneous determination of source parameters. Subsection 2 presents a processing package for on-line analysis of data from small-aperture arrays. Subsection 3 is a study on optimization of seismic array configuration. Subsection 4 and 5 describe the upper mantle seismic heterogeneities beneath Fennoscandia and Eastern Europe. Subsection 6 describes a work for mapping the crustal structure and thickness in the coastal areas of southern Norway and the general features of the Moho near and in the Oslo Graben. Subsection 8 is a noise study at various sites in Finland, in northern Norway and in southeastern Norway.

II. OPERATION OF ALL SYSTEMS

II.1 Detection Processor (DP) Operation

There have been 178 breaks in the otherwise continuous operation of the NORSAR online system within the current 6-month reporting interval. The SPS is still working well and has caused only 0.8% downtime. A software problem that occurred in conjunction with stopping the online transmission of data via the ARPA net caused almost half of the downtime in the period. The uptime percentage for the period is 91.9 as compared to 89.0 for the previous period.

Fig. II.1.1 and the accompanying Table II.1.1 both show the daily DP downtime for the days between 1 October 1981 and 31 March 1982. The monthly recording times and percentages are given in Table II.1.2.

The breaks can be grouped as follows:

a)	SPS malfunction	20
b)	Stops related to possible program errors	74
c)	Maintenance stops	5
d)	Power jumps and breaks	5
e)	Hardware problems	61
f)	Magnetic tape and disk drive problems	11
g)	Stops related to system operation	2

The total downtime for the period was 353 hours and 38 minutes. The mean-time-between-failures (MTBF) was 1.3 days as compared with 0.9 days for the previous period.
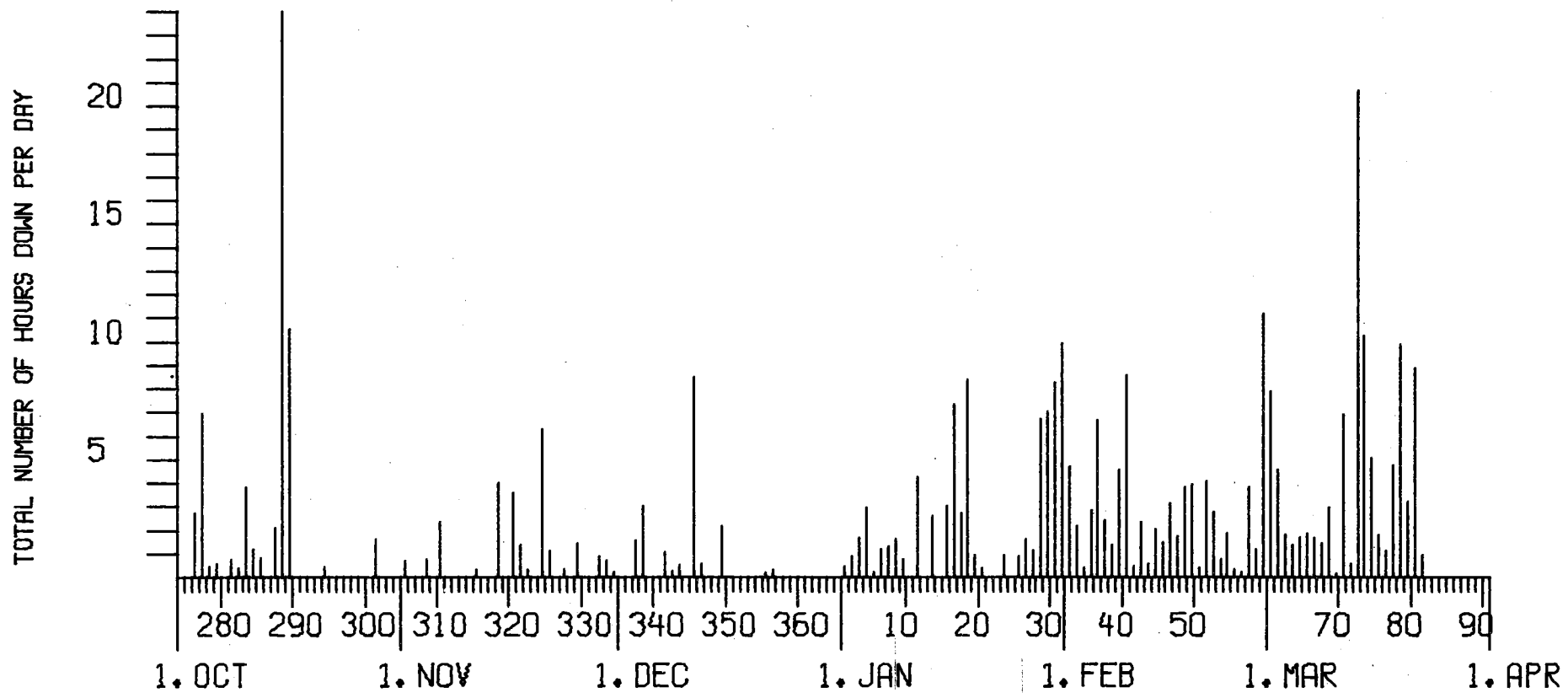
J. Torstveit

Fig. II.1.1   Detection Processor downtime in the period 1 October 1981 –
31 March 1982.

LIST OF BREAKS IN DP PROCESSING THE LAST   HALF-YEAR

DAY	START		STOP		COMMENTS..........	DAY	START		STOP		COMMENTS..........
276	21	17	24	0	POWER BREAK	332	15	6	15	58	CPU ERROR
277	0	0	6	57	POWER BREAK	333	22	0	22	41	CPU ERROR
278	8	30	8	38	CPU ERROR	334	13	8	13	18	CPU ERROR
278	10	51	11	2	CPU ERROR	305	20	0	20	41	CPU ERROR
278	14	24	14	31	CPU ERROR	308	10	8	10	54	CE WORK
279	10	24	10	33	CPU ERROR	310	4	7	6	26	CPU ERROR
279	12	58	13	23	CPU ERROR	315	11	9	11	28	CPU ERROR
281	21	5	21	49	CPU ERROR	318	8	18	12	18	CPU ERROR
282	7	24	7	47	CPU ERROR	320	1	45	4	58	CPU ERROR
283	2	6	5	42	CPU ERROR	320	10	40	10	55	CPU ERROR
283	12	59	13	11	CPU ERROR	320	23	54	24	0	CPU ERROR
284	16	35	17	44	CPU ERROR	321	0	0	0	37	CPU ERROR
285	7	53	8	22	MT ERROR	321	10	47	10	57	CPU ERROR
285	10	53	11	13	DISC ERROR	321	15	23	15	58	CPU ERROR
287	21	53	24	0	CPU ERROR	322	13	18	13	36	CPU ERROR
288	0	0	24	0	CPU ERROR	324	1	18	7	36	CPU ERROR
289	0	0	10	15	CPU ERROR	325	10	49	11	56	MT ERROR
289	10	37	10	52	MT ERROR	327	12	6	12	25	MT ERROR
294	22	31	22	56	CPU ERROR	329	19	55	21	19	CPU ERROR
301	16	22	17	57	CPU ERROR	332	15	6	15	58	CPU ERROR
305	20	0	20	41	CPU ERROR	333	22	0	22	41	CPU ERROR
308	10	8	10	54	CE WORK	334	13	8	13	18	CPU ERROR
310	4	7	6	26	CPU ERROR	337	9	51	11	22	CE WORK
315	11	9	11	28	CPU ERROR	338	4	30	7	30	CPU ERROR
318	8	18	12	18	CPU ERROR	341	6	24	7	25	CPU ERROR
320	1	45	4	58	CPU ERROR	342	8	19	8	34	CPU ERROR
320	10	40	10	55	CPU ERROR	343	15	42	16	12	CPU ERROR
320	23	54	24	0	CPU ERROR	345	7	0	14	58	CPU ERROR
321	0	0	0	37	CPU ERROR	345	15	32	16	3	CPU ERROR
321	10	47	10	57	CPU ERROR	346	12	22	12	56	PROG ERROR
321	15	23	15	58	CPU ERROR	349	8	39	10	50	CE WORK
322	13	18	13	36	CPU ERROR	355	9	10	9	22	SPS ERROR
324	1	18	7	36	CPU ERROR	356	8	42	9	0	CPU ERROR
325	10	49	11	56	MT ERROR	1	0	0	0	25	RESET(NEW YEAR)
327	12	6	12	25	MT ERROR	2	19	24	20	17	SPS ERROR
329	19	55	21	19	CPU ERROR	3	0	46	1	42	SPS ERROR

Table II.1.1   (page 1 of 3)

LIST OF BREAKS IN DP PROCESSING THE LAST   HALF-YEAR

DAY	START	STOP	COMMENTS...........	DAY	START	STOP	COMMENTS...........
3	4 49	5 32	SPS ERROR	35	2 8	4 5	PROG ERROR
4	5 39	7 16	PROG ERROR	35	21 27	22 21	CPU ERROR
4	10 38	11 59	SPS ERROR	36	1 54	7 43	PROG ERROR
5	10 19	10 30	SPS ERROR	36	7 47	7 56	SPS ERROR
6	2 35	3 33	SPS ERROR	36	12 6	12 45	SPS ERROR
6	9 18	9 31	MT ERROR	37	3 6	4 1	PROG ERROR
7	13 49	15 6	POWER BREAK	37	17 30	19 0	PROG ERROR
8	18 46	20 13	SPS ERROR	38	9 0	10 21	PROG ERROR
8	23 52	24 0	PROG ERROR	39	3 23	7 26	PROG ERROR
9	0 0	0 44	PROG ERROR	39	12 26	12 56	PROG ERROR
11	4 40	8 55	SPS ERROR	40	1 31	2 22	SPS ERROR
13	4 45	7 19	SPS ERROR	40	4 54	12 38	SPS ERROR
15	7 34	7 51	MT ERROR	41	10 46	11 12	SPS ERROR
15	9 31	9 51	MT ERROR	42	8 52	9 42	PROG ERROR
15	21 37	24 0	SPS ERROR	42	18 15	19 26	POWER BREAK
16	0 0	7 18	SPS ERROR	42	19 45	20 5	CPU ERROR
17	21 19	24 0	PROG ERROR	43	10 0	10 34	PROG ERROR
18	0 0	8 23	PROG ERROR	44	6 35	8 36	PROG ERROR
19	15 5	15 13	SPS ERROR	45	1 4	1 49	PROG ERROR
19	23 0	23 47	PROG ERROR	45	21 33	22 16	PROG ERROR
20	14 16	14 40	SPS ERROR	46	9 43	12 52	PROG ERROR
23	7 2	7 57	SPS ERROR	47	5 47	7 30	PROG ERROR
25	10 26	11 18	PROG ERROR	48	0 47	2 3	PROG ERROR
26	4 15	5 34	PROG ERROR	48	20 35	23 9	PROG ERROR
26	14 30	14 46	POWER BREAK	49	16 32	18 17	PROG ERROR
27	6 16	7 21	PROG ERROR	49	19 38	21 50	SPS ERROR
28	0 36	7 19	PROG ERROR	50	11 55	12 18	PROG ERROR
29	0 41	7 27	PROG ERROR	51	3 40	7 3	PROG ERROR
29	16 2	16 17	CPU ERROR	51	20 16	20 56	PROG ERROR
30	10 11	11 6	PROG ERROR	52	7 46	10 17	PROG ERROR
30	16 40	24 0	PROG ERROR	52	23 46	24 0	PROG ERROR
31	0 0	9 54	PROG ERROR	53	0 0	0 29	PROG ERROR
32	2 12	6 52	PROG ERROR	53	13 26	13 40	PROG ERROR
33	0 43	1 34	PROG ERROR	54	3 13	4 19	PROG ERROR
33	21 36	22 54	PROG ERROR	54	11 5	11 36	PROG ERROR
34	10 23	10 45	PROG ERROR	54	14 2	14 14	DISK ERROR

Table II.1.1 (page 2 of 3)

LIST OF BREAKS IN DP PRCCESSING THE LAST   HALF-YEAR

DAY	START		STOP		COMMENTS...........	DAY	START		STOP		COMMENTS...........
55	9	50	9	59	PROG ERROR	75	0	0	0	14	PROG ERROR
55	13	10	13	21	DISK ERROR	75	16	45	18	19	PROG ERROR
56	7	49	8	0	PROG ERROR	76	6	20	7	26	PROG ERROR
57	3	40	7	28	PRCG ERROR	77	2	23	7	7	PRCG ERROR
58	22	51	24	0	CPU ERROR	78	0	8	9	59	PROG ERROR
59	0	0	0	3	CPU ERROR	79	0	50	1	47	PROG ERROR
59	4	1	13	52	PROG ERROR	79	13	33	15	48	PROG ERROR
59	15	46	16	22	CPU ERROR	80	1	49	10	8	PRCG ERROR
59	21	31	22	8	PROG ERROR	80	23	28	24	0	PRCG ERROR
60	0	31	7	15	CPU ERROR	81	0	0	0	16	PROG ERROR
60	16	56	18	6	PROG ERROR	81	13	41	14	22	PROG CHANGE
61	4	49	7	44	PRCG ERROR						
61	10	18	11	6	CPU ERROR						
61	11	45	12	34	CPU ERROR						
62	2	26	3	12	CPU ERROR						
62	22	12	23	13	PRCG ERROR						
63	13	37	14	57	CPU ERROR						
64	2	48	3	37	PROG ERROR						
64	9	34	10	24	POWER BREAK						
65	1	56	2	46	PROG ERROR						
65	21	1	22	2	PROG ERROR						
66	12	31	12	50	PROG ERROR						
66	18	29	19	19	PROG ERROR						
66	19	50	20	21	PRCG ERROR						
67	7	38	8	52	CE WORK						
67	14	57	15	9	PROG ERROR						
68	8	17	11	13	PROG ERROR						
69	10	52	11	1	PRCG ERROR						
70	2	35	7	58	PROG ERROR						
70	21	15	22	46	PROG ERROR						
71	7	52	8	26	DISK ERROR						
72	3	22	16	30	CPU ERROR						
72	16	30	24	0	TEST RUN 4331						
73	0	0	10	12	TEST RUN 4331						
74	3	7	7	22	PROG ERROR						
74	23	14	24	0	PRCG ERROR						

*** NUMBER OF BREAKS =   174
*** MEAN TIME BETW. FAILURES =   1.1 DAYS
*** NUMBER OF UPTIME INTERVALS =   175

Table II.1.1   (page 3 of 3)

Month	DP Uptime (hrs)	DP Uptime (%)	No. of DP Breaks	No. of Days with Breaks	DP MTBF* (days)
Oct	687.85	92.5	17	14	1.6
Nov	695.85	96.6	18	15	1.5
Dec	725.98	97.6	11	10	2.5
Jan	667.28	89.7	31	25	0.9
Feb	592.68	88.2	47	28	0.5
Mar	644.98	86.7	34	22	0.8
	4014.62	91.9	158	114	1.3

*Mean-time-between-failures = (Total uptime/No. of up intervals)

TABLE II.1.2

Online System Performance
1 October 1981 - 31 March 1981

II.2 Event Processor Operation

In Table II.2.1 some monthly statistics of the Event Processor operation are given:

	Teleseismic	Core Phases	Sum	Daily
Oct 81	186	53	239	7.7
Nov 81	174	59	233	7.8
Dec 81	243	120	363	11.7
Jan 82	292	58	350	11.3
Feb 82	168	42	210	7.5
Mar 82	231	55	286	9.2
	1294	387	1681	9.2

TABLE II.2.1

B. Kr. Hokland

II.3 NORSAR Data Processing Center (NDPC) Operation

Data Center

The operator function is now being carried out by four persons on a weekly shift turn. In addition a fifth person steps in for a day or two when necessary, as they all have another main function to cover.

J. Torstveit

II.4 Array Communication

Table II.4.1 reflects the performance of the communications system throughout the reporting period.

In addtion to ordinary irregularities in the communication system itself, the table also reflects other prominent conditions, such as:

-       CTV power failure (high voltage and ripple)
-       Line switching between the SPS and the Modcomp processor
-       Maintenance visits
-       Tests from NDPC.

In October 02B was affected by unwanted interference signals in the communications system. Ordinary operation resumed 21 October. After periods with reduced reliability, 02C cable between Lillehammer and Hornsjø was rerouted 12 October. 28 October the 02C subarray was switched to the Modcomp computer for test recording. 04C was affected week 43, noise caused spikes in the data and B/C loop was found inoperative. Attempts to replace'the modem and SLEM power supply did not improve the operation, as errors were still detected in the modem test mode (C-loop). A communications test 28 October proved satisfactory operation without errors.

In November most of the subarrays were affected. 10 November 01A and 01B modems situated at the NDPC lost power. 01B was also affected 11-13 November due to high ICW error rate, and 25 November due to scheduled NTA maintenance work. 02B went down 6 November and remained down until 11 November, probably due to loss of power.

After a period in ordinary operation 02C was again switched to Modcomp 3 November. 18 and 19 November the same subarray was affected by a broken air cable in the Mesnalien area. Week 48 we found the ICW's returned from 04C. The reason was a short circuit between two pairs of wires causing an artificial loop to be set up.

In December three arrays were affected. 02C, as usual used in Modcomp test connnections, was brought back in ordinary operation week 49. 03C was down 4,5,6 and 7 December for unknown reasons. A planned operation at the NTA Elverum affected 03C and 04C 16 December.

January. The operation at Elverum 16 December where NTA phased in a new system had a bad affect with respect to 03C, as they were not able to restore the original condition on the communications system. From 11 January 02C was used more or less continuously in connection with Modcomp tests. Errors were observed in connection with 04C ICW's, but the number of errors was less than 50 and did not affect or deteriorate the data.

Also in February 02C was switched to Modcomp most of the time. 8 February 01B was affected due to low level (-40.0 dB). 01A was affected week 8 due to low level toward the subarray. 01B and 03C were affected the same week, causing ICW and ODW outage, respectively.

March. As in the previous months 02C was frequently used in connection with Modcomp tests. Also 04C and 03C were used, but for shorter periods. 03C was affected by suspected cable fault in the Rena area. To restore the B/C loop feature, a card was replaced in the 03C modem.

Table II.4.2 indicates distribution of outages with respect to the individual subarrays. The table also reflects (by asterisks) weeks when some or all subarrays have been affected simultaneously.

II.5   The ARPA Subnetwork

In October and November periods with reduced line quality were observed.

II.6 The Terminal Interface Message Processor (TIP)

In connection with installation of a power distribution panel the TIP power was removed for 4-5 hours 10 November. Week 50 the NORSAR connection to the ARPA network and TIP was terminated. System power was turned off 21 December.

O.A. Hansen

Sub-Array	OCT (4) (5.10-1.11)		NOV (4) (2-29.11)		DEC (5) (30.11-3.1.82)		JAN (4) (4.1-31.1)		FEB (4) (1-28.2)		MAR (5) (1.3-4.4)		AVERAGE ½ YEAR	
	>20	>200	>20	>200	>20	>200	>20	>200	>20	>200	>20	>200	>20	>200
01A	–	–	0.1	1.1	–	0.3	0.1	0.2	0.1	12.6	0.1	0.2	–	2.4
01B	–	0.3	0.1	6.3	0.5	0.1	–	0.5	–	1.2	0.1	0.2	0.1	1.4
02B	5.5	16.2	0.1	18.5	–	0.1	–	–	0.3	0.1	0.1	0.2	1.0	5.8
02C	10.3	8.2	–	93.3	0.1	10.6	0.2	53.9	–	77.2	–	53.6	1.7	49.5
03C	–	0.3	0.5	0.6	–	5.6	0.1	3.8	–	22.4	–	34.6	0.1	11.2
04C	1.6	28.5	2.6	1.7	2.6	0.8	2.2	0.5	0.2	0.4	–	0.5	1.5	5.4
06C	–	0.9	–	0.1	–	–	3.5	0.6	0.7	0.4	1.0	0.7	0.7	0.4
AVER	2.5	7.8	0.5	17.4	0.4	2.5	0.9	8.5	0.2	16.3	0.2	12.8	0.7	10.8
LESS	02B 02C	02B,02C 04C	02B 03C		02C		02C 03C		02C 03C		02C 03C		02C 03C	
	0.3	0.4	1.6		1.0		2.1		0.2		0.2		2.2	

TABLE II.4.1

Communications (degraded performance >20/outages >200)
Figures in per cent of total time. Month four or five weeks, as indicated.

Week/	Subarray/per cent outage						
Year	01A	01B	02B	02C	03C	04C	06C
41/81	–	–	36.1	2.8	0.7	0.2	0.9
42	–	0.7	–	2.1	–	1.2	–
43	0.2	0.3	28.7	–	0.2	93.4	0.2
44	–	0.4	–	28.1	0.3	19.2	2.5
45	–	–	42.3	73.2	0.1	–	–
46	4.3	22.2	31.2	100.0	0.4	3.1	0.1
47	–	–	–	100.0	1.2	0.4	–
48	0.4	3.1	0.4	100.0	0.9	3.3	0.3
49	–	2.4	–	50.6	11.9	0.1	–
50	0.1	0.1	0.1	2.2	15.6	0.4	0.1
51	–	–	–	–	0.4	0.9	–
52	1.5	0.2	0.4	0.1	0.1	0.3	0.1
53	–	–	–	–	–	2.2	–
1/82	0.1	–	–	2.1	–	0.6	–
2	–	–	–	37.5	0.6	0.4	0.1
3	–	2.2	–	95.2	9.1	0.5	–
4	0.6	–	–	80.9	5.5	0.4	2.2
5	3.6	1.8	–	100.0	15.9	0.3	1.0
6	46.1	0.1	0.1	8.7	8.9	0.7	0.7
7	–	0.1	0.1	100.0	7.6	0.6	–
8	0.6	2.8	0.3	100.0	57.4	0.1	0.1
9	1.0	1.0	1.0	25.0	71.4	0.9	0.9
10	–	–	0.1	–	71.4	–	–
11	–	–	–	91.7	11.4	1.2	0.4
12	–	–	–	100.0	11.1	0.6	–
13	–	–	–	51.2	7.5	–	2.2

TABLE II.4.2

III. IMPROVEMENTS AND MODIFICATIONS

III.1 NORSAR On-line System using IBM 4331/4341 and Modcomp Classic

The IBM VM/SP operating system is designed for fast terminal access to
many simultaneous users, and therefore given highest priority to handle
terminal interrupts. This priority is built into the system and may not
be changed. This means that a real-time system, i.e., the Modcomp to IBM
communication, running under VM/SP control, may be disturbed by use of
a terminal.

For the design of our new DP system, this means that we should not allow
any terminal use on this machine, since this may cause loss of interrupts
from the Modcomp communication controller. For NORSAR this is no problem,
since all control of the DP system is done via shared disk access between
the 4331 and 4341 computer. Moreover, the Max4 operating system from
Modcomp will later this year support their IBM channel interface which
was originally in our design for the SPS substitution. If a change to this
kind of interface is done, the transfer of data may be at a speed of 512
Kbytes rather than 230 Kbit per second. The earlier reported loss of data was
not mainly due to the above discussed terminal access priority in VM/SP, but
due to the handling of error checking in the IBM bisync protocol (CRC-check).
We can now conclude that with correct CRC generation on Modcomp, and no extra
users on the IBM system, we have no loss of data in the transmission between
Modcomp and IBM.

We have the following elements of the on-line system in operation:
Communication with Modcomp. Receiving high rate data block, subarray beam data
and NORESS data o.k. Transferring FS/FRS data and manual status to Modcomp o.k.
No loss of data.

Recording of data on disk. o.k. We have direct access using a system where the
time of the data determines which block to use, i.e., given time of data,
number of disks and disk size we can read the data directly with no search.
The data is available to the 4341 by shared-disk access. A total of 36 hours
may presently be recorded on the allocated disks. The space allocated for
DPX's may cover one year of DPX data.

Detection processing. So far no problems have been encountered. A few hours
of full array detection test have been performed, and a concluding test running
over several days will be performed in a short time.

Tape recording. o.k. 6250 BPI is used and one tape will cover 12 hours of NORSAR
and NORESS data. Presently a blocking of 9 seconds of NORSAR data is used.
The new tape format will be compatible with present high rate tapes, except for
a longer blocking than the present 2.0 seconds block and the presence of 'NA'-
records (NORESS).

Calibration status. All software necessary to transmit any FS/FRS is o.k. Manual
status setting is o.k. All calibration/status commands are executed on the
4341 computer. Simulation of EOC alternate telemetry commands is not yet
implemented.

Experimental operation console (EOC). The EOC now displays seismometer data in
a scrolling manner, i.e., the traces will move out of the screen at one edge as
new data is coming in on the opposite edge of the screen.

The hardware we have on the 4341 system is capable of displaying only 'frozen'
pictures (i.e., Tektronix 618 screens attached to the IBM 3277 graphic attach-
ment). The plot software developed may display any number of short period data
from NORSAR and/or NORESS. Default option will plot the latest 50 seconds
recorded, or any time interval that is present on the on-line disk. A program
for displaying long period data is also developed. The same program may handle
calibration/status commands so that you may initiate calibration of an instru-
ment and 'immediately' see the sine waves displayed on the graphics screen.

All EOC commands end up in FS/FRS sequences or DOF1/DOF2, and so far we
have capabilities of initiating FS/FRS commands. The full simulation of
all EOC commands will be implemented as needed.

Note: Although we have designed a system where new terminals will be used
        for status, calibration and plotting, we might also consider attaching

the EOC to the 4341 computer directly. The software involved in using
the EOC as it is used in the old system will in that case need to be
developed, a task which we have not yet looked into.

So far we may conclude that all EOC operations except alternate telemetry
commands have replacements in the new system.

SPS substitution (Modcomp). The software developed on the Modcomp turned out
to have a too high overhead to run 7 subarrays (7 BSC lines) simultaneously.
The subcontractor has now reprogrammed the ICW and ODW-handling, and 7-subarray
operation has been tested successfully. Some further refinements are being
worked on.

The new TOD unit had to be returned to the factory due to occasional
jumps in time (1 second time jumps). Meanwhile we are using the oldest
TOD for Modcomp tests. This has given some problems to the communications
stability, but will be resolved as soon as the new unit is back from the
factory.

Event processing. So far we have a system for copying data intervals from on-
line disk to EPX files using the DPX list for time intervals. The FASTEP
program is changed to use disk files rather than tape input. Event processing
is not fully automated but the basic programs for event processing from on-
line data is available now.

Conclusion. The present software on Modcomp does perform the SPS tasks, and
may replace SPS as it is. However, a few improvements should be done.

The present software on IBM 4331 does perform the recording, detection and
calibration/status tasks. Some minor changes are necessary to include
message, DPX and EPX transmission to Modcomp and further to AFTAC. Due to
terminal priority in VM/SP it is not practical to use the 4331 for other

users together with the on-line system, and a stand-alone program would
be sufficient to run the new DP system. This would make more disk space
available.

The present software on IBM 4341 can now perform the tape recording, on-line
plotting, calibratin and status (array monitoring) task, and event processing
may be done. The latter needs some more organization to use the disk space
effectively for EPX data.

The next reporting period should give the performance of and experiences
with the new system.

J. Fyen

III.2 Field instrumentation and facilities

Refer to Table III.2.1 for changes of the array stations up to the end of
May 1982. An analog line from 06C CTV was operational as of 8 October 1981
carrying eight of the NORESS channels (see Table III.4.1 in Torstveit, 1981).
The channels are digitized and recorded by the MODCOMP computer. The Landrover
was replaced with a new Mercedes 300D at the end of the reporting period and
fully operational in May.

A. Kr. Nilsen

Reference

Torstveit, J. (ed.) (1981): Semiannual Technical Summary, 1 Apr - 30 Sep 1981,
    NORSAR Scientific Report No. 1-81/82.

Subarray Normally	Instr. No. within SA	Ch. No. on NORSAR Data Tape	Time of change		
			10/30/81	02/15/82	05/25/82
01A	1	1		Standard HS-10 seism. (1)	
(1)	2	2		_"_ (2)	
	3	3		_"_ (3)*	
	4	4		30 dB att. ch. up (4)	
	5	5		_"_	
	6	6		_"_	
01B	1	7			
(2)	2	8			
	3	9			
	4	10			
	5	11			
	6	12			
02B	1	13			
(3)	2	14			
	3	15			
	4	16			
	5	17			
	6	18			
02C	1	19			
(4)	2	20			
	3	21			
	4	22			
	5	23			
	6	24			

* Cable broken, dead

TABLE III.2.1

Status of NORSAR SP instruments recorded on data tape.
(Page 1)

Subarray Normally	Instr. No. within SA	Ch. No. on NORSAR Data Tape	Time of Change 10/30/81	Time of Change 02/15/82	Time of Change 05/25/82
03C (5)	1	25			−
	2	26			−
	3	27			−
	4	28			−
	5	29			8 Hz filter out (6)
	6	30			4.75 Hz filter in
04C (6)	1	31			
	2	32			
	3	33			
	4	34			
	5	35			
	6	36			
06C (7)	1	37	Previous ch. 01B01*		
	2	38	" 06C02*		
	3	39	" 06C04*		
	4	40	" 01B03*		
	5	41	" 01B04*		
	6	42	" 01B05*		

* NORESS data

TABLE III.2.1
(Page 2)

IV.   FIELD MAINTENANCE ACTIVITY

In this section a very brief review of the field maintenance is given. There is little change from previous periods and the error rate and maintenance activity are normal. Two new stations are operative in the subarray 02B area and radio transmitted to NORSAR field maintenance center at Stange and recorded on a Kinemetrics PDR-2 digital seismic recorder.

Maintenance Visits

Table IV.1 gives the number of visits to the NORSAR subarrays during the reporting perod. The average number of visits to each subarray is 2.4, not including the work with the new stations in the 02B area.

Subarrays	01A	01B	02B	02C	03C	04C	06C/NORESS	Total
No. of Visits	5	4		1	2	1	4	17

TABLE IV.1

Number of visits to the NORSAR subarrays including NORESS
in the period 1 Oct 1981 – 31 Mar 1982

Preventive Maintenance Projects

The preventive maintenance work of the NORSAR array instrumentation and facilities listed in Table IV.2. The adjustments are corrections of characteristics within the tolerance limits.

Unit	Action	No. of Actions
Seismometer	MP adjust (in field)	14
	FP -"- -"-	1
Line Termination	Adjustment of channel gain (SP)	2
Amplifier	DC offset (SP)	1
Emergency Power	Battery and charger check	5
Cleaning of CTV		1

TABLE IV.2

Preventive maintenance work in the period
1 October 1981 - 31 March 1982

Corrective Maintenance

The corrective maintenance comprising the required adjustment and replacements is given in Table IV.3.

Unit	Characteristics	SP		LP	
		Repl.	Adj.	Repl.	Adj.
Seismometer	FP (in field)				14
	MP (in field)				6
	MP/FP (at NDPC)				43
	RCD				2
Seismometer Ampl. RA/5, Ithaco	Gain			1	
	Protection card	1			
	Taperpin block	1			
Line Termination Amplifier	Gain				
	DC offset	1			
EPU		1			
SLEM					
Mux	Spikes	1			

TABLE IV.3

Total number of required adjustments and replacements of NORSAR field equipment in the period 1 October 1981 - 31 March 1982.

Power Breaks, Cable Breakages, Communications Faults

One power break required action of our field technicians, and broken cables
to 01B 04,05 were repaired. Two communication faults were corrected by our
field crew.

Array Status

As of 31 March 1982 the following channels had out-of-tolerance conditions:
01A03; 02B04; 03C06,V; 04C V; NORESS 06,09; 06C V,NS.
Channels with nonstandard conditions are:

01A	04	Attenuated 30 dB
01A	06	8 Hz Filter
02B	06	-"-
04C	06	-"-
06C	01,03-06	NORESS (02 is placed in LPV)

A.Kr. Nilsen

ABBREVIATIONS

CTV	–	Central Terminal Vault
DC	–	Direct current
EPU	–	External Power Unit
FP	–	Free period
LP	–	Long period
MP	–	Mass position
MUX	–	Multiplexer
NDPC	–	NORSAR Data Processing Center
NORESS	–	NORSAR Experimental Small-Aperture Subarray
RCD	–	Remote centering device
SLEM	–	Seismic short and long period electronics module
SA	–	Subarray
SP	–	Short period

V. DOCUMENTATION DEVELOPED

Asudeh, I., 1982: Seismic structure of Iran from surface and body-wave
     data. Submitted for publication.

Doornbos, D.J.: Seismic source spectra and moment tensors. Submitted for
     publication.

Gjøystdal, H., J.E. Reinhardsen & B. Ursin, 1981: Travel time and wavefront
     curvature calculations in inhomogeneous layered media with curved
     interfaces. Paper presented at SEG meeting, Los Angeles, October 81.

Nysæter, A., 1981: Quadratic versus linear envelope beamforming for seismic
     event detection. NORSAR Tech. Rep. 3/81, NTNF/NORSAR, Kjeller.

Reinhardsen, J.E., 1981: Dynamic ray-tracing in complex three-dimensional
     media. Tech. Rep. 1/81, NTNF/NORSAR, Kjeller.

Torstveit, J., 1981: Semiannual Technical Summary, 1 Apr - 30 Sep 1981.
     NORSAR Sci. Report 1-81/82, NTNF/NORSAR, Kjeller.

Tryggvason, K., 1981: 3-D mapping of the Iceland hot spot. NORSAR Tech. Report
     4/81, NTNF/NORSAR, Kjeller.

VI.   SUMMARY OF TECHNICAL REPORTS/PAPERS PREPARED

VI.1   Seismic source spectra and moment tensors

The quantification of seismic sources (e.g., scalar moment or magnitude),
the determination of source size (e.g., corner frequency methods), and
the determination of radiation pattern (e.g., fault plane solutions),
are procedures which usually proceed separately and use different parts
of the seismic spectrum. Of course, the various source parameters are
not independent of one another, and they are often related through semi-
empirical rules (Kanamori and Anderson, 1975). There would be obvious
advantages if source parameters could be determined simultaneously. The
seismic moment tensor represents both scalar moment and radiation pattern,
but applications are restricted to what may be regarded as point sources.
In principle it is possible to remove this restriction by extending the
representation to moment tensors of higher degree (Backus, 1977), and
as described in the previous semiannual report, in practice it is
possible to estimate moment tensors up to degree two (Doornbos, 1982a).
At this stage, however, a long-period approximation is still implied,
and spectral information above the corner frequency cannot be used in
the present procedure.

In a more recent attempt to reconcile the information from long- and
short-period data (Doornbos, 1982b) it was shown that when the source
spectrum is expanded in powers of frequency, the coefficient of the
n'th power is a linear function of the n'th moment tensor:

$$F(\underline{\zeta},\omega) = 1 - i\omega\underline{\zeta}^T\underline{F}_{(1)} - \tfrac{1}{2}\omega^2\underline{\zeta}^T\underline{\underline{F}}_{(2)}\underline{\zeta} + \ldots \tag{1}$$

where $\underline{F}_{(1)}$ and $\underline{\underline{F}}_{(2)}$ are the moment tensors of degree 1 and 2, respectively,
and $\underline{\zeta}$ is a 4-dimensional slowness vector:

$$\underline{\zeta} = (\gamma_1/c, \ \gamma_2/c, \ \gamma_3/c, 1)^T$$

where c is wave velocity and γ_ℓ a direction cosine of the wave. It should
be noted that equation (1) gives the moment tensor expansion of a scalar
source function $f(\underline{\xi},\tau)$ which is relative to the moment tensor density of
the source by

$$\dot{m}_{jk}(\underline{\xi},\tau) \simeq M_{jk}f(\underline{\xi},\tau) \tag{2}$$

and M_{jk} is the moment tensor of degree zero.

The form (1) explicitly shows the low-frequency approximation by moments of low degree, and suggests suitable ways of extrapolation. In extrapolating to higher frequencies the implied spectral assumption restricts the source model to a particular class, and in Fig. VI.1.1 several possibilities are compared on the basis of a typical triangular earthquake source pulse. The models included are among others ω-square:

$$H(\underline{\zeta},\omega) = \left\{1+\tfrac{1}{2}\omega^2\underline{\zeta}^T\hat{\underline{F}}_{(2)}\underline{\zeta}\right\}^{-1} \exp\left\{-i\omega\underline{\zeta}^T\underline{F}_{(1)}\right\} \tag{3}$$

and Gaussian:

$$N(\underline{\zeta},\omega) = \exp\left\{-\tfrac{1}{2}\omega^2\underline{\zeta}^T\hat{\underline{F}}_{(2)}\underline{\zeta} - i\omega\underline{\zeta}^T\underline{F}_{(1)}\right\} \tag{4}$$

Here, $\hat{\underline{F}}_{(2)}$ is measured with respect to the source's 'center of gravity' in space and time $(\hat{\underline{\xi}}_o,\hat{\tau}_o)$, for which $\underline{F}_{(1)} = 0$. The model has 20 parameters, involving moments of degree zero, one and two. Model-dependent constraints can reduce this number to that employed in other methods. The models lead to simple expressions for the displacement field and the total radiated seismic energy, and they can be made to satisfy certain general properties of observed far-field spectra, including the corner frequency shift of P waves with respect to S waves.

Moments of degree zero represent the final static source parameters, which are usually obtained in a point source approximation from long-period data. A mislocation of the source gives rise to moments of degree one. They determine the phase spectrum in the spectral model, and their determination is equivalent to the classical source location problem by travel time analysis. The source's spatial and temporal extent give rise to moments of degree two. They control the spectral bandwidth and its variation with take-off angle and wave velocity, and their determination

corner frequency methods of determining source dimensions. Although
solutions for the moments of different degree are not independent, it
should often be possible to obtain initial estimates of the moments of
degree zero (linear inversion), one and two (linear or nonlinear inversion)
consecutively, from long- and shortperiod data or more precisely, from
data in at least two frequency bands.

Inversion methods based on this model are being developed to obtain
estimates of scalar moment, seismic energy, source size and stress drop,
from long- and short-period SRO/ASRO data. It is also found that the
following points need further study: (1) The presently employed digital
SRO response can be small in crucial parts of the excitation spectrum of
commonly observed sources (m_b roughly in the range 5-6). (2) Frequency
dependence of Q appears to be needed in source retrieval from long-
and short-period data. (3) Short-period amplitude anomalies can signifi-
cantly affect the source estimates. Points (2) and (3) corroborate the
results of others.

D.J. Doornbos

References

Backus, G.E. (1977): Interpreting the seismic glut moments of total degree
two or less. Geophys. J.R. astr. Soc. 51, 1-25.

Doornbos, D.J. (1982a): Seismic moment tensors and kinematic source para-
meters. Geophys. J.R. astr. Soc. 69, 235-251.

Doornbos, D.J. (1982b): Seismic source spectra and moment tensors. Phys.
Earth Planet. Inter., issue on 'Earthquake algorithms', in press.

Kanamori, H. and D.L. Anderson (1975): Theoretical basis of some empirical
relations in seismology. Bull. Seismol. Soc. Amer. 65, 1073-1095.
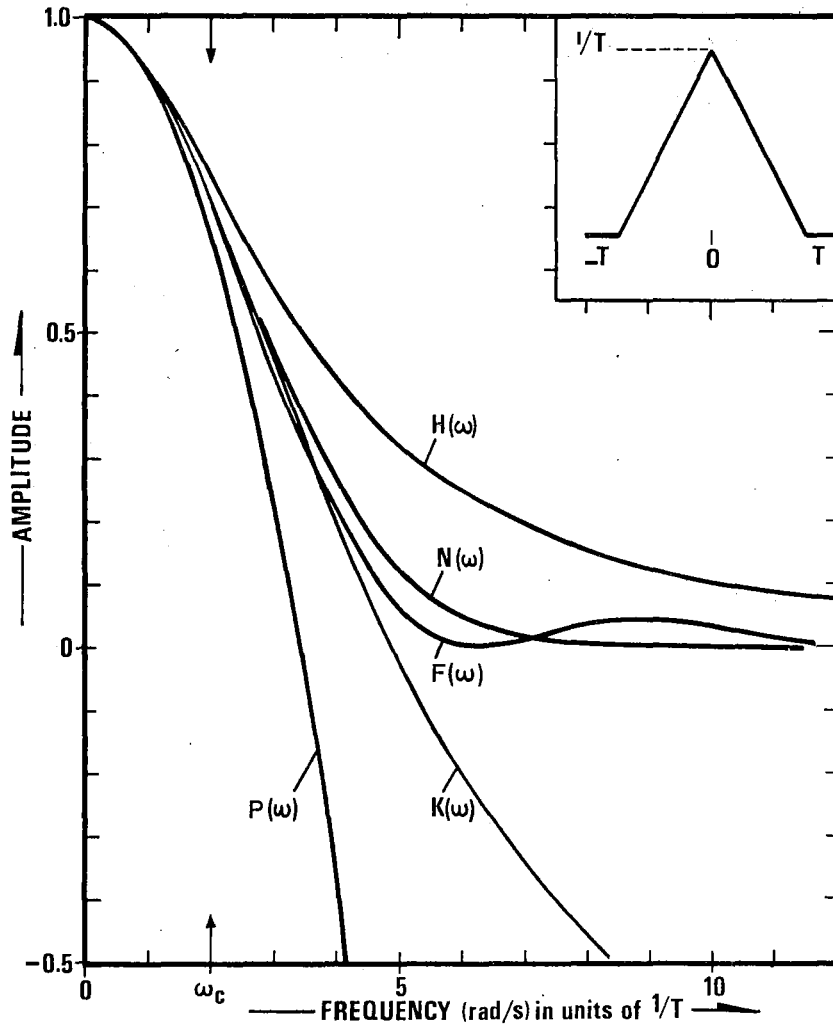
Fig. VI.1.1 Spectral approximations to triangular source pulse (see inset)
with amplitude spectrum $F(\omega)$ and corner frequency ω_c.
$H(\omega)$: ω-square model (eq. (3)); $N(\omega)$: Gaussian model (eq. (4)).
$P(\omega)$ and $K(\omega)$ are a parabolic and a rational approximation,
not mentioned in the text.

VI.2   A processing package for on-line analysis of data from small-aperture arrays

A Regional 'ON-line' Array Processing Package (RONAPP) has been developed and tested on off-line data from the small-aperture NORESS array at NORSAR. This array consists of 12 sensors spaced with distances up to about 2 km, and the processing package automatically detects and locates regional seismic events in the distance range from a few kilometers to the maximum propagation range of regional S-type waves (Sn or Lg). The package consists of a conventional STA/LTA detector, a phase identification procedure based on phase velocity, and a location procedure based on observed travel time differences and a common azimuth between the observed primary and secondary phases. In the following we give some details on the detection and detection processing procedures and a description is given of the phase association scheme adopted. Finally some processing results are shown and discussed.

Detection and detection processing

In the present version, the detector works on either a vertical beam or a single channel and with a number of filters. For each filter, STA/LTA is computed and compared successively against two different thresholds. Three blocks of data (presently with 4 sec in each) are always kept in memory, with the detection performed in the middle block. If no detection is declared, the first block is dropped, a new one is brought in, and the procedure is repeated. In case of one or more detections in the current block, data within a certain time window around each detection are written on disk, estimates of refined arrival time and signal frequency are obtained, and a wavenumber analysis is performed following a proper pre-filtering. This gives estimates of phase velocity, azimuth and power for each detection, which together with arrival time and frequency constitutes the essential part of a detection record. The detection procedure is continuous and not dependent on the block structure. A block diagram outlining the detection and detection processing procedures is shown in Fig. VI.2.1.

Phase association and event location

Following each processed detection, an event location is performed if
the last detection is identified as an S-type wave (phase velocity below
6 km/s), and also a P-wave (phase velocity above 6 km/s) has been detected
within an appropriate azimuth range. Distance is taken from an S-P travel
time table. An intricate procedure is developed to allow for several
detections within the P and S coda, to keep track of 'used' and 'unused'
detections, and to identify locations that override previous ones.

The identification of phase type according to phase velocity being above
or below 6 km/sec is justified from 'manual' wavenumber analysis of NORESS
data from well-identified phases (Mykkeltveit & Ringdal, 1981).

The automatic phase association and location procedure assumes in its
present version that the largest secondary arrival detected is an Lg
phase. The block diagram in Fig. VI.2.2 gives the details.

The main problem in the location procedure, however, is the correct
identification of the type of secondary arrival (in practice Sn or Lg)
which is associated with P. It is not possible from our wavenumber analysis
to distinguish between Sn and Lg on the basis of phase velocities alone.
Unless other objective criteria can be found, it will be necessary to
invoke region-dependent information on the general occurrence of secondary
seismic phases. Regional events within 12-15° recorded by NORESS are domi-
nated by strong Lg waves, propagating at a fairly constant group velocity
of 3.5 km/sec. Exceptions are events in Central Europe, England, Scotland
and western part of the North Sea, from which Sn is the dominating phase
and Lg is very weak if at all seen. The strong attenuation of Lg is
probably an effect of larterally varying structures along paths to NORESS
from these regions. Events from or close to the North Atlantic Ridge
show the same characteristics. A detailed investigation of regional
propagation characteristics within 15° of NORSAR and correlation with
gross geological features is in progress.

Experience with the processing package

The processing package has been tested on a number of data intervals from the
12-sensor NORESS array. Our experience so far can be summarized as follows:
The on-line automatic processing package provides location results as good
as those previously reported by Mykkeltveit and Ringdal (1981) for manual
analysis of NORESS data, provided:

a)   proper positioning of time window for f-k analysis

b)   the automatically determined frequency for the f-k analysis must corre-
     spond to peak in signal spectrum

c)   data to be subjected to f-k analysis must be properly prefiltered

d)   assumptions inherent in the automatic phase association are valid.

Points b) and c) above ensure reliable phase velocity and azimuth results
from the f-k analysis, while d) is an obvious requirement for proper
location. Fig. VI.2.3 serves as an illustration of the importance of the
positioning of the time window for f-k analysis. This figure gives the
results from a sliding window analysis, where phase velocity and azimuth
results are plotted for windows of length 2.5 sec shifted 0.6 sec at a time.
Each time window has been subjected to f-k analysis for 9 frequencies in
the range 3-5 Hz and results plotted (at the time interval midpoint) cor-
respond to the frequency with maximum power.

Fig. VI.2.3 shows that azimuth and phase velocity estimates for this high
signal-to-noise-ratio event are comparatively stable around the onset times
for the main phases. Azimuth values derived from time intervals in the codas,
on the other hand, fluctuate around the expected value. For this event,
however, all P and Lg coda detections (two for each phase) are associated
with lower power than the phase onset detections, which are marked in the
figure. Consequently, our association and location procedures work well
in this case.

Epicentral distance is determined from the first P and the strongest Lg-
type detection via the time difference between these two detections. A good
estimate of distance relies upon the assumption that the amplitude maximum

in the Lg wave train can be associated with a constant group velocity
of 3.5 km/s. This assumption has been justified by the testing performed
so far.

Fig. VI.2.4 shows the data for the 12 NORESS channels and the vertical
beam for a presumed mining explosion located by the Finnish network to
the Finland-U.S.S.R. border at a latitutde of about 61°N. The arrows
indicate the four detections by our processing package and results from
f-k analysis. Besides the P and Sn detections, there are two Lg detections;
the f-k plot shown corresponds to the strongest one. This example shows
that our detection and location procedure works also for a fairly modest
signal-to-noise-ratio event.

Although more refinement and testing are still needed, we have finalized
the basic design for a package that, when finished, should be suitable for
implementation within the framework of a low-power, microcomputer-based
system.

S. Mykkeltveit
H. Bungum
F. Ringdal

References

Mykkeltveit, S. and F. Ringdal (1981): Phase identification and event
     location at regional distance using small-aperture array data. In:
     Identification of Seismic Sources - Earthquake or Underground
     Explosion (eds. E.S. Husebye and S. Mykkeltveit). Reidel Publ. Co.,
     Dordrecht.

```
┌─────────────────────────┐
│   Detection and         │
│ detection processing    │
└─────────────────────────┘
```

```
┌──────────────────────────┐        In buffer:
│   Fill up 1st block      │        3 blocks of data
└──────────────────────────┘        Block size: 4 sec

┌──────────────────────────┐
│   Initialize detector    │
└──────────────────────────┘

┌──────────────────────────┐
│   Fill up 2nd block      │◄──────────────────┐
└──────────────────────────┘                   │

┌──────────────────────────────┐               │
│ Detection processing, 2nd block│              │
│   Filtering, STA/LTA analysis  │             │
└──────────────────────────────┘               │

          ╱ Any ╲                    ┌────────────────────┐
         ╱ detection? ╲──── No ─────▶│ Replace 1st block  │
         ╲            ╱               │    with 2nd        │
          ╲        ╱                  └────────────────────┘
             Yes

┌──────────────────────────┐
│    Fill up 3rd block     │
└──────────────────────────┘

┌──────────────────────────┐
│  Find refined onset time │
│  Find signal frequency   │
└──────────────────────────┘

┌──────────────────────────┐
│       Filtering          │
│      FK-analysis         │
└──────────────────────────┘

┌──────────────────────────┐
│  Write detection record  │
└──────────────────────────┘

┌──────────────────────────┐
│    Phase association     │
└──────────────────────────┘

┌──────────────────────────┐
│   Replace 2nd block      │
│      with 3rd            │
└──────────────────────────┘
```
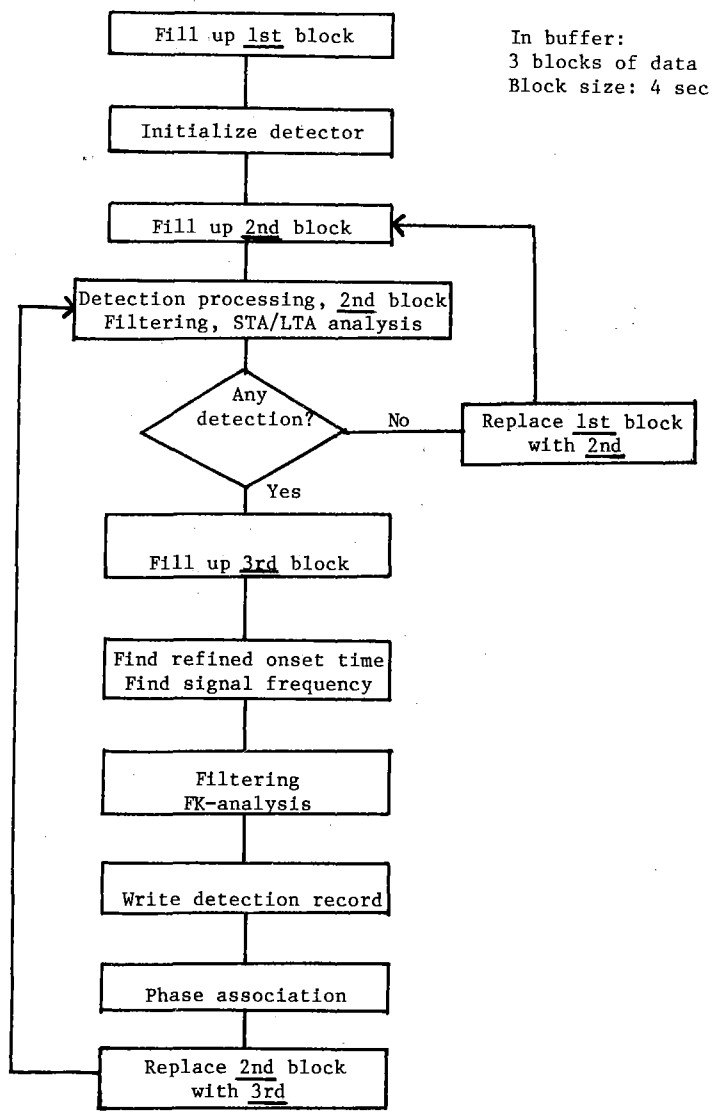
Fig. VI.2.1   Block diagram showing the detection and detection processing
in RONAPP.
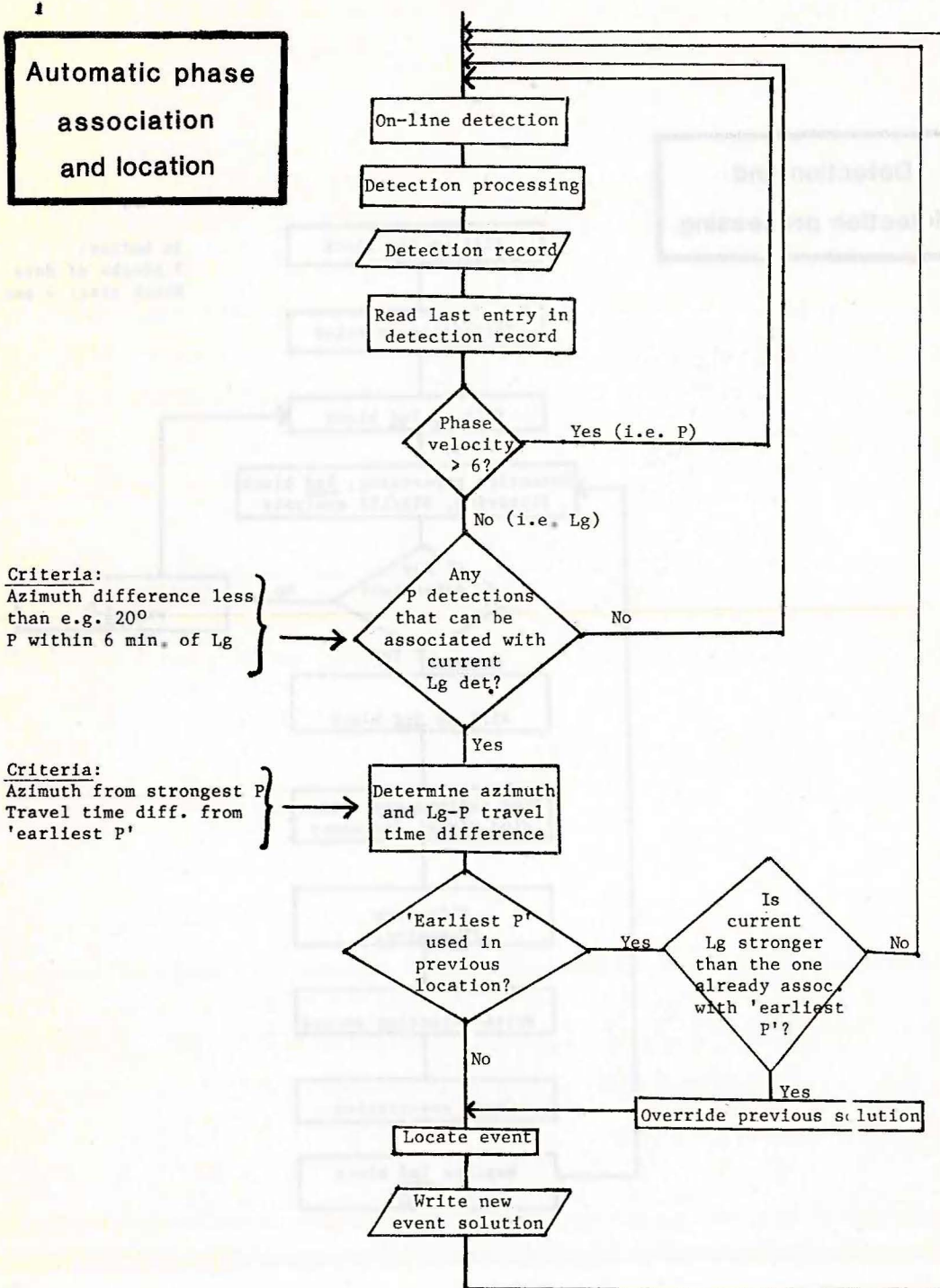
Fig. VI.2.2   Block diagram with details on phase association and location
procedure in RONAPP.
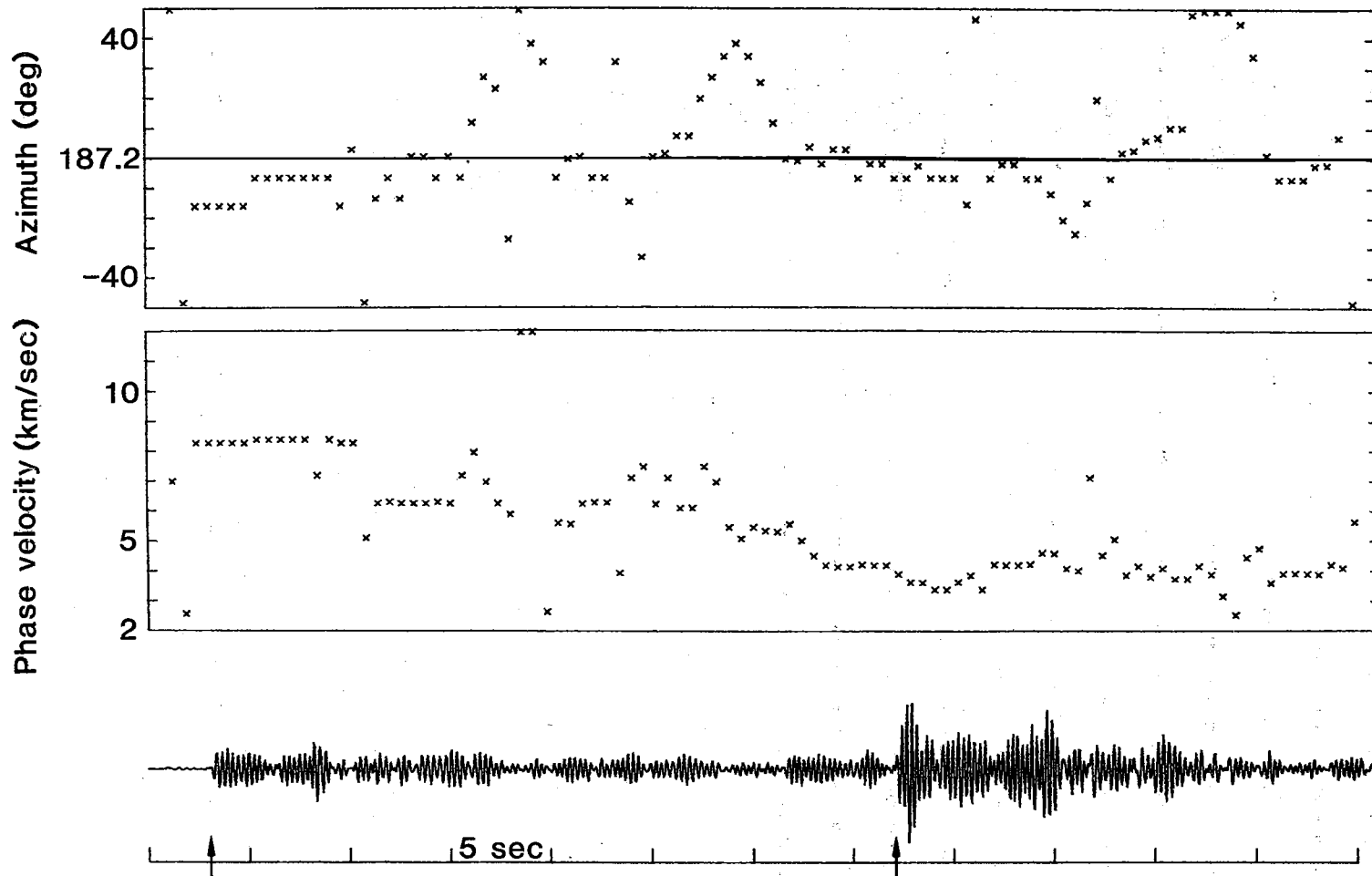
Fig. VI.2.3 Results from sliding window analysis of NORESS data from a presumed explosion in the sea at a distance of 260 km, direction south. Data for one of the NORESS channels are shown, and arrows indicate the detections used in phase association and location. The line in the azimuth diagram shows the azimuth according to the epicenter solution by the Scandinavian network of seismic stations. The uncertainty of this solution in terms of azimuth from NORESS may be as large as 5-10 degrees.
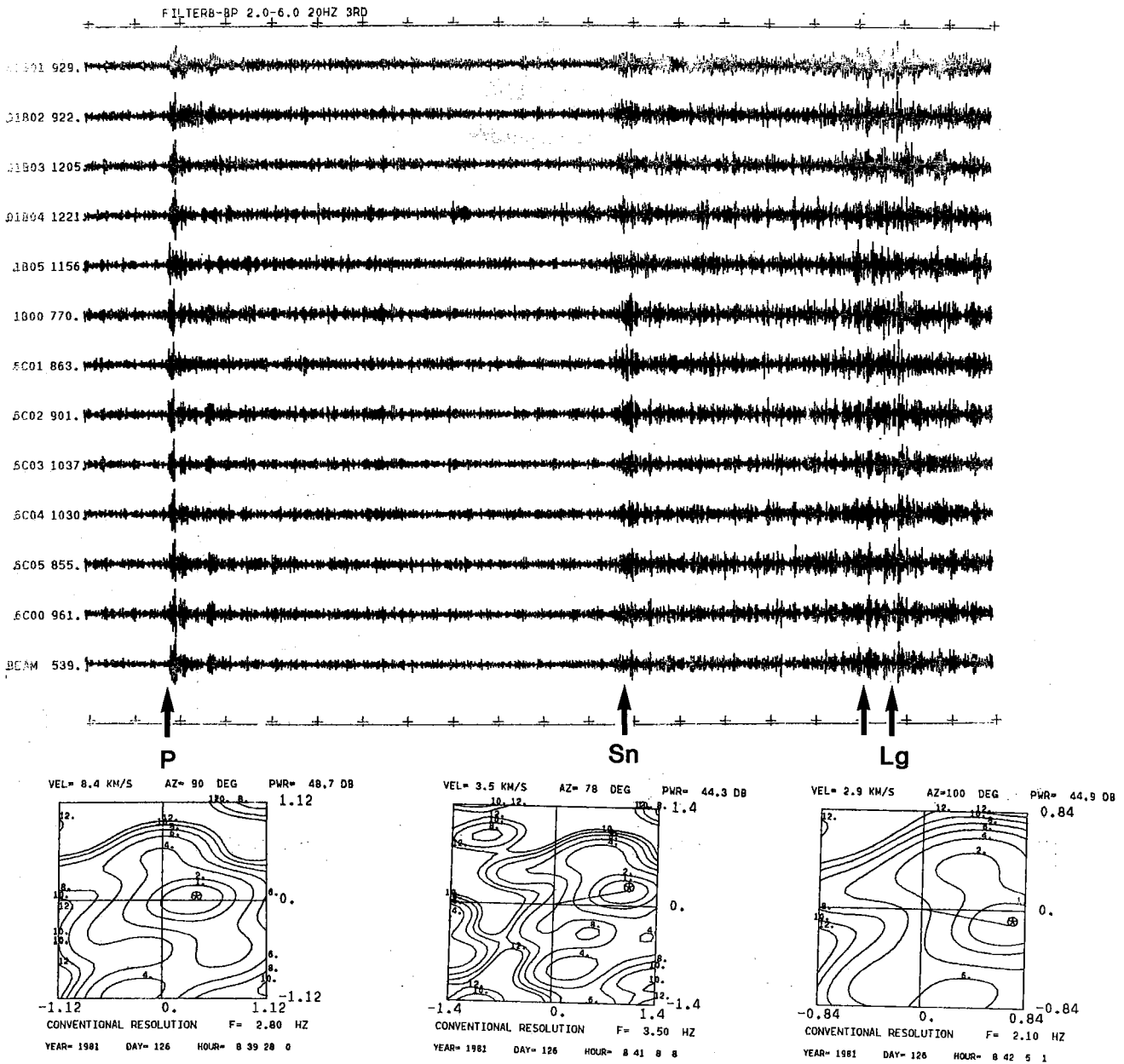
Fig. VI.2.4 NORESS data (and vertical beam) for a presumed mining explosion in the Finland/U.S.S.R. border region. There are four detections and f-k plots for three of them are shown.

VI.3   Seismic array configuration optimization

The seismological concept of arrays emerged from the nuclear test ban
negotiations in Geneva in 1958 when the need for improved capability
to study weak seismic events was clearly recognized. Over the years
many kinds of array systems have been installed in many countries, but
LASA and NORSAR remained the unique ones; unique in terms of their sizes
(apertures of the order of 200 and 100 km, and number of instruments
once 588 and 198, respectively), and because dedicated data centers
were made an integral part of these arrays.

In Norway a miniarray termed NORESS (NORSAR Experimental Small Subarray)
has recently been installed within the NORSAR array itself and is shown in
Fig. VI.3.1. The motivation for this undertaking is to provide data for
optimum design of a complete array system for surveillance of events
at regional distances. This is the research topic dealt with in this
section.

Signal and noise structure

An essential aspect of the array design is a priori assumptions regarding
the statistical structure of signal and noise. Generally speaking, the
array response when 'steered at' the signal, should be small at wavenumbers
characteristic of the noise. Intersensor spacings would then correspond
to maximum correlation for the signal and a minimum for the noise.
A common assumption has been that of equal signals and uncorrelated
noise beyond a critical space lag, and for sufficiently large intersensor
spacing the array design criteria are trivially met. However, observations
usually contradict these assumptions, and our optimization procedure
will be based on actually observed signal and noise correlations using
NORESS recordings.

Signal correlations

A major objective of our work was to derive an optimum layout for detect-
ing events at regional distances, so signal correlations were measured for
phases identified as Pg, Pn and Lg for the 5 events listed in Table VI.3.1,

all within 12° of NORESS. A record section of Event 5 is displayed in
Fig. VI.3.2, signal correlations in Fig. VI.3.3. We see that the Pg
phase exhibits high correlation values for all frequency bands and
sensor separations displayed. The Lg phase on the other hand correlates
rather poorly in the higher frequency ranges. The results for the Pn
phase show increasing correlation with frequency, which reflects a
corresponding peak in the signal spectrum around 4 Hz.

Noise correlation

Selected noise records, including both summer and winter conditions,
were subjected to correlation analysis, and the results obtained are
also given in Fig. VI.3.3. The most notable feature here is that the
correlation curves consistently have a negative minimum before tending
to zero, which is rated significant. This observational fact, easily
missed when noise similarity is expressed via the coherency measure,
is consistent with a model of propagating noise, as demonstrated
by Mykkeltveit et al (1982).

In Fig. VI.3.4 we show the theoretical correlation function for noise
with a uniform wavenumber spectrum in the range $(2\pi)^{-1}$ to $5 \cdot (2\pi)^{-1}$ c/km.
This wavenumber range would be appropriate for typical Rayleigh wave
phase velocities (3-4 km/s) in a frequency range roughly 0.6 to 3 Hz,
or typical body wave phase velocities (above 6 km/s) at frequency
above 1 Hz. The curve is reasonably close to the observed curve which is
taken from Fig. VI.3.3 and testifies to the importance of propagating
noise at the Rayleigh wave velocities, even at relatively high frequencies.
This is in accord with the results of wavenumber analysis, although higher
phase velocities typical of body waves are also observed.

The optimization procedure

Let signal to noise ratio gain by beamforming be expressed by

$$G^2 = \sum_{ij} w_i w_j c_{ij} / \sum_{ij} w_i w_j \rho_{ij} \qquad (1)$$

where c_{ij} is the signal correlation between sensors i and j, ρ_{ij} similarly describes the noise correlation and w_i are sensor weights. In the common beamforming practice at arrays, $w_i=1$. Then, since c_{ii} = ρ_{ii} = 1, equation (1) can be rewritten in the more common form:

$$G^2 = \frac{1+(N-1)\bar{c}}{1+(N-1)\bar{\rho}} \tag{2}$$

where $\bar{c}$, $\bar{\rho}$ describe average signal and noise correlations for an N sensor array. Alternatively, it is possible to use weighted beamforming (e.g., Christoffersson and Husebye, 1974), and the optimum gain function for noise suppression is simply the reciprocal maximum likelihood estimate of noise power (c.f. Boverie and Gregg, 1971):

$$G'^2 = \sum_{ij} \rho_{ij}^{-1}$$

where ρ_{ij}^{-1} form the inverse correlation matrix of the noise. Our reasons for optimizing G rather than G' are that (i) G with unit weights reflects the common beamforming practice at arrays, (ii) G contains both noise and signal, (iii) G is more stable with respect to variations in the estimate of noise correlation.

The gain is a nonlinear function of the sensor coordinates, and for more than three sensors we obtained a maximum of G by applying a standard rapid descent method (Fletcher and Powell, 1963) to analytic approximations of the correlation functions in Fig. VI.3.3. As might be expected, the optimum configuration is strongly determined by the position of the noise correlation minimum, but for relatively poorly correlating signals like Lg, the slope of the signal correlation curves is also important. Since these features are frequency dependent (see Fig. VI.3.3), different optimum geometries will result for different frequency bands. A compromise is to optimize a combination of the gains in different frequency bands.

Figs. VI.3.5 and VI.3.6 show examples of the gain averaged over the
5 frequency bands of Fig. VI.3.3, where the optimization was done se-
quentially from 3 to 20 sensors. Whereas the gain for Lg is near the
standard factor $\sqrt{N}$ (in amplitude), which results from the assumption
of identical signals and uncorrelated noise, the gain for Pg is system-
atically higher.

Our final configuration with 20 sensors for Pg gives a gain 4 dB above $\sqrt{N}$.
As demonstrated in Fig. VI.3.7, together with the gains in individual
frequency bands. For example, in Fig. VI.3.7 we have included the optimum
geometry for the frequency band 1.6-4.0 Hz, with clearly reduced intersensor
spacings as compared to the averaged geometry for the 5 frequency bands.
Corresponding results for Lg are given in Fig. VI.3.8; here the optimum
geometry for frequency band 1.6-4.0 Hz has larger dimension than the
averaged geometry.

Obviously, the optimum 3 sensor array should form an equilateral triangle,
with intersensor spacing close to the noise correlation minimum. From
Figs. VI.3.5 and VI.3.7 it is clear that for Pg the same optimum intersensor
spacing dominates the array geometry for a larger number of sensors. An
illustrative example is the optimum geometry for 20 sensors (Fig.
VI.3.7), with two pairs of sensors near the center of the array. This
is interpreted as indicating the importance of these positions, with a
maximum number of other sensors at optimum distance. For Lg (Figs. VI.3.6
and VI.3.8), similar observations can be made with regard to number of
sensors and array dimension, the principal difference being that, due
to reduced signal correlations, intersensor spacings and array dimension
are also reduced. More generally, the trade-off between the effect of
increased number of sensors and increased array dimension should be
considered for limiting the final number of sensors in the regional
array. Another important point is that the array performance inevitably
would depend on phase type and frequency, but 'worst case' events can
be considerably improved by flexible weighting schemes.

Although the main scope of our study has been array design for sur-
veillance of regional events, the methodology applied is not limited
to this task. For example, our array concept is also the likely basic
subarray unit in a large aperture ('teleseismic') array, in which case
the 'optimum' main/side lobe strategy for deployment of subarray units
as once used for LASA and NORSAR would be adequate. A more comprehensive
presentation of the work synthesized above is given by Mykkeltveit et al
(1982).

S. Mykkeltveit
K. Åstebøl
D.J. Doornbos
E.S. Husebye

References

Boverie, B. and W.D. Gregg (1971): A signal detectability approach
    to optimizatin of the geometry of distributed aperture (array) receivers.
    I.E.E.E. Trans. Ant. Prop. AP-19, 22-30.

Christoffersson, A. and E.S. Husebye (1974): Least squares signal estimation
    techniques in analysis of seismic array recorded P-waves. Geophys. J.R.
    astr. Soc. 38, 525-552.

Fletcher, R. and M. Powell (1963): A rapidly convergent descent method for
    minimization. Comput. J. 6, 163-168.

Mykkeltveit, S., K. Åstebøl, D.J. Doornbos and E.S. Husebye (1982): Seismic
    array configuration optimization. Manuscript submitted for publication.

Date	Origin time	Location		Local Magnitude
06 Nov 1980	14.53.02	59.5°N	10.7°E	2.1
25 Nov 1980	02.39.49	58.4°N	13.7°E	2.4
29 Nov 1980	20.42.16	51.2°N	18.5°E	3.5
26 Feb 1981	17.43.53	60.3°N	15.9°E	2.1
01 Mar 1981	05.08.16	62.8°N	6.2°E	2.7

Table VI.3.1

Local events used in this study.
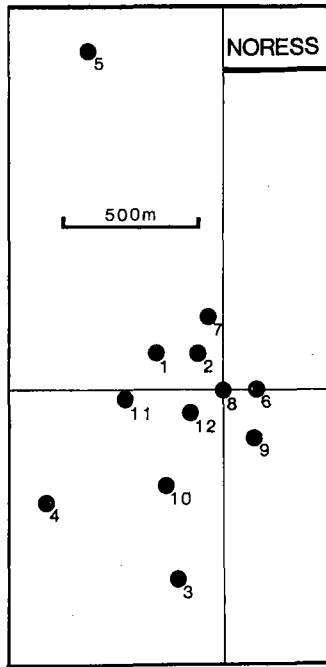
Fig. VI.3.1 Geometry of the 12-element NORESS array. All sensors are equipped with 4.75 Hz antialiasing lowpass filters.
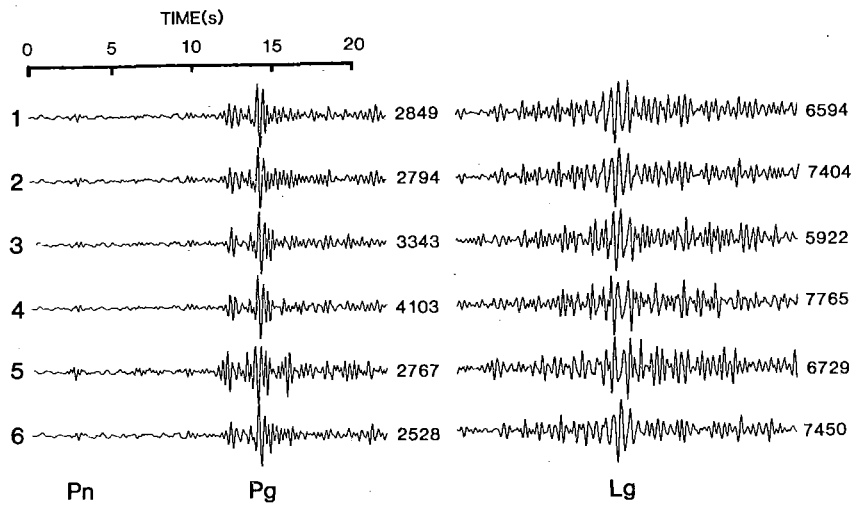
Fig. VI.3.2   NORESS records (channels 1-6 in Fig. VI.3.1) for event 5 in Table VI.3.1. For each phase, correlation measurements are made from 2 sec of data around the phase maximum. All traces are normalized, numbers to the right give scaling factors. The gap between Pg and Lg is 29 sec.
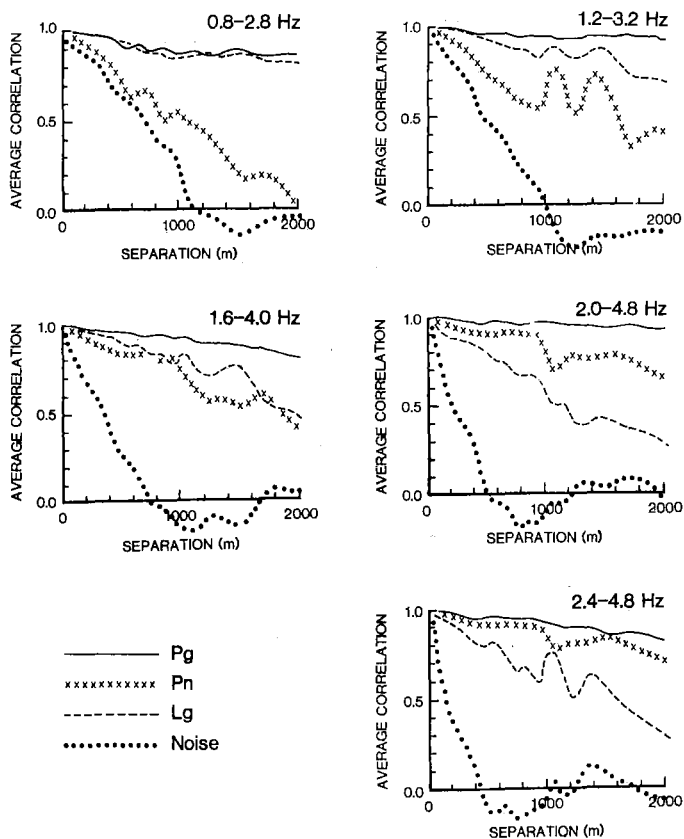
Fig. VI.3.3　Correlation vs distance for Pg, Pn, Lg and noise at NORESS
for the five frequency ranges indicated. Each curve is based
on measurements from 66 combinations of sensor pairs.
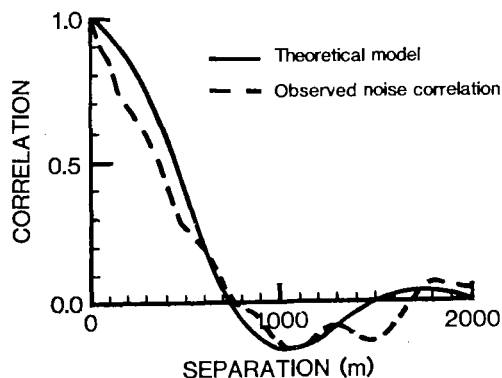
Fig. VI.3.4　Theoretical correlation function for noise with a uniform
wavenumber spectrum in the range $(2\pi)^{-1}$ to $5(2\pi)^{-1}$ c/km. The
observed noise correlation function (dashed line) is reproduced
from Fig. Vi.3.3 (frequency range 1.6-4.0 Hz).
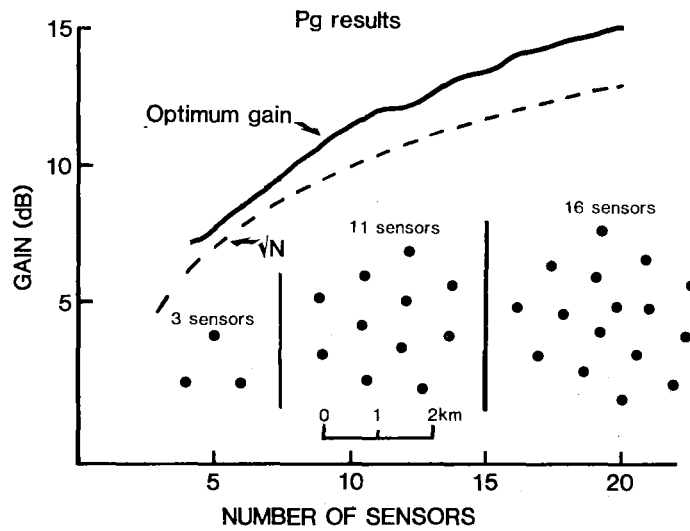
Fig. VI.3.5   Gain for the Pg phase as a function of number of sensors for
geometries derived from our optimization procedure. The starting
geometry for 3 sensors along with resulting geometries for 11
and 16 sensors are shown. The gain is an average over the 5
frequency bands in Fig. VI.3.3.
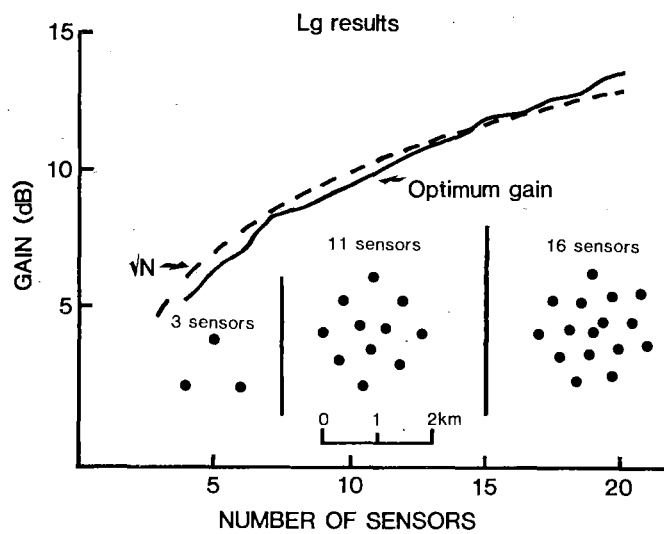
Fig. VI.3.6   Same as Fig. VI.3.5, but for the Lg phase.

Pg results
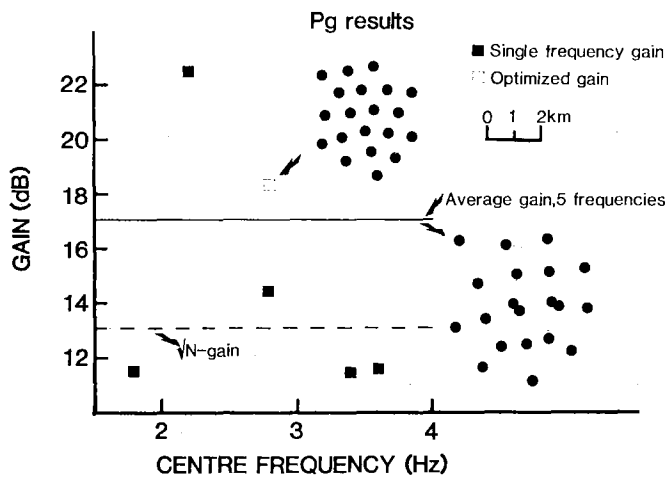
Fig. VI.3.7 Pg gains for an optimized 20-element array. The lower right
geometry is optimum when the gain function is expressed as the
sum of 5 individual gain functions for the frequency bands
shown in Fig. VI.3.3. This geometry gives different gain for
each band, as indicated by the 'single frequency gains'. The
geometry derived from a 'mulitple' gain function is different
from that based on a single frequency band. This is demonstrated
by reoptimizing the lower right configuration for the frequency
band centered at 2.8 Hz resulting in a net gain of 4 dB and a
new geometry as shown. The exceptionally large gain for the
frequency band centered at 2.2 Hz reflects the pronounced
negative noise correlation observed here (see Fig. VI.3.3).
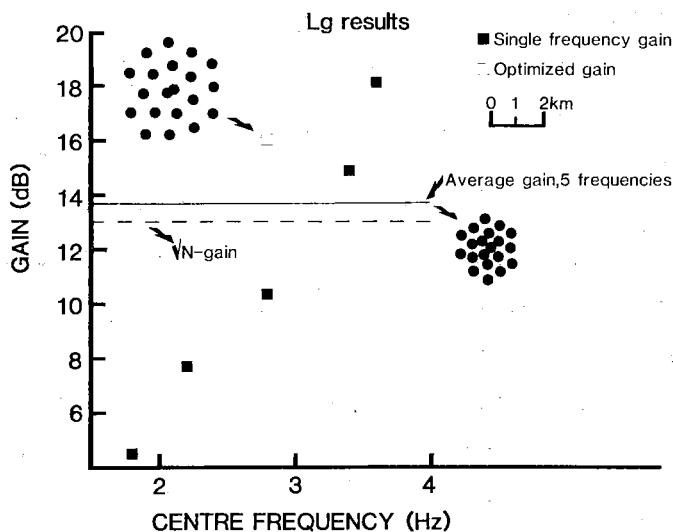
Fig. VI.3.8   Lg gains for an optimized 20-element array. The geometry to the right is optimum when the gain function is expressed as the sum of 5 individual gain functions in the frequency bands given in Fig. VI.3.3. This geometry gives different gains for each band, as indicated by the 'single frequency gains'. The optimum geometry derived from a 'multiple' gain function is different from that based on a single frequency band. This is demonstrated by reoptimizing the lower right configuration for the frequency band centered at 2.8 resulting in a net gain of nearly 6 dB and a new geometry as shown. The higher frequency ranges are seen to dominate the 'average' geometry.

VI.4 Upper mantle seismic heterogeneities beneath Fennoscandia

Three-dimensional seismic mapping of the upper mantle beneath Fennoscandia
(Baltic Shield) using an ACH-type of inversion technique in combination
with P-wave travel time residual observations from the local seismograph
network gave the following results. The central parts of the Baltic Shield
are characterized by relatively high seismic velocities down to approximately
300 km. Those parts of the shield most affected by the Caledonide orogeny
exhibit relatively low velocities particularly in the uppermost 100 km
depth interval. The lower part of the upper mantle (300-600 km) does not
exhibit pronounced seismic velocity anomalies and in this respect is in
contrast to results from similar studies in regions subjected to neotectonic
processes like parts of central and southeastern Europe. The seismic
anomaly pattern in the presumed thickened lithosphere is in quantitative
agreement with similar ones derived from surface wave dispersion analysis
and inversion of electrical measurements. The general orientation of
these anomalies coincides with that of the glacial uplift. A comprehensive
description of this work can be found in a recent paper by Husebye and
Hovland (1982).

E.S. Husebye
J. Hovland, Univ. of Oslo

Reference

Husebye, E.S. and J. Hovland (1982): On upper mantle seismic heterogeneities
    beneath Fennoscandia. Tectonophysics, in press.

VI.5 Upper mantle heterogeneities beneath Eastern Europe

P-wave travel time residuals for seismograph stations in Eastern Europe
as reported by ISC for the years 1964-77 were used for constructing a
seismic image of upper mantle heterogeneities in the network region.
For the depth range 0-100 km, dominant tectonic features like the Pannonian
Basin and the Aegean Sea and Western Turkey correlate well with pronounced
velocity lows which appear to extend down to a 300 km depth. The velocity
anomaly patterns in the depth intervals 300-500 km and 500-600 km are
broadly similar but quite different from those of shallower depths. The
observed seismic heterogeneities are briefly discussed in terms of large-
scale tectonic and geophysical (heat-flow) characteristics of Eastern
Europe. A comprehensive description of this work can be found in a recent
paper by Hovland and Husebye (1982).

J. Hovland, Univ. of Oslo
E.S. Husebye

Reference

Hovland, J. and E.S. Husebye (1982): Upper mantle heterogeneities beneath
    Eastern Europe. Tectonophysics, in press.

VI.6   A North Sea - Southern Norway seismic crustal profile

Introduction

During the last decade numerous seismic profiling investigations have been
carried out in Fennoscandia and a relatively large number of crustal
models have been derived. There is considerable inconsistency concerning
the number of crustal layers and the associated velocity distributions
as reported by various authors. The reason for this is probably a combina-
tion of real crustal variations, relatively poor sampling densities and
the non-uniqueness inherent in the interpretation of refraction seismic
data.   Consequently, as a Cambridge group was carrying out a refraction
experiment across the North Sea in the summer of 1980, we took the oppor-
tunity to expand the shot-firing scheme in order to obtain a densely
sampled land profile (CANOBE) in southern Norway. The profile was posi-
tioned in a north-easterly direction, away from the line of shots off
the southern coast and running parallel to the western border of the
Oslo Graben as shown in Fig. VI.6.1.

In this section we present an interpretation of the high quality records
obtained along the densely sampled CANOBE profile. Synthesis of P-wave
amplitudes and travel times, assuming a laterally varying structure,
constitutes the basic tool for mapping the crustal structure and thickness
in the coastal areas of southern Norway and the general features of the
Moho near and in the Oslo Graben.

Field work and preparation of the data

The CANOBE project, its name derived from the participating institutions
Cambridge University, NORSAR and Bergen University, took place between
the 26th of July and the 4th of August 1980. A total of 13 recording
instruments were available. Four explosions from a coinciding Cambridge
North Sea refraction project (N2-N5 in Fig. VI.6.1) were located to the
east of the Central Graben in the North Sea, and were used for the land-
recording in Norway.   In addition the Royal Norwegian Navy provided
several tons of AMATOL in the form of torpedo warheads and a coast guard
ship to fire shots H1-H6 also marked in Fig. VI.6.1.

The recording scheme consisted of seven legs (Fig. VI.6.1), one per shot, each comprising 13 mobile stations. Legs 1 to 3 had a sensor spacing of 4 km, legs 4 to 6 a 6 km spacing and leg 7 a spacing of 5 km. Leg 7 transected the Oslo Graben just north of Oslo while the main line ran across the Precambrian rocks to the west, extending into the NORSAR array siting area. Five NORSAR subarrays (01A, 02C, 03C, 04C, 06C) recorded the shots continuously, thus enabling the main line distance range to be extended to about 515 km.

The initial record sections were filtered between 0.2 and 15 Hz. Fig. VI.6.2 shows the record section corresponding to the main line for shots N5 and H1-H5, reduced by 8 km/s. The NORSAR array records, from 450 km onwards, have been low pass filtered at 4.75 Hz sampling rate 20 Hz. True amplitudes are multiplied by distance in the record sections. The spectra for typical records in this section are found to have dominant frequencies within 2.5 to 3.5 Hz.

Interpretation of the CANOBE data

Although the quality of the data and the relatively dense sensor spacing along the profile provide and excellent basis for interpretation we are somewhat encumbered by lack of observations for the first 70 km of the profile and by the absence of a reversed coverage. This being said, the interpretational results are as follows:

Interpretation of the main line section assuming lateral homogeneity

Starting with P_g and P_n velocities taken from the record section (Fig. VI.6.2) and Moho depths in the expected range of 30-35 km, theoretical time-distance curves were computed until a satisfactory fit with the data was achieved. A prominent feature in the record section are the large amplitudes of secondary arrivals at about 186 km, apparently part of the P_MP branch. While modelling the data on the basis of travel times a velocity-depth configuration was established which produces a focusing effect near the outer cusp in the triplication (Fig. VI.6.3). The outer cusp is made to terminate at 250 km by introducing a velocity gradient of 0.025 s^{-1} in the depth interval 5.5 km to 25 km, and an increasing velocity gradient

down to 32.5 km where a velocity of 8.1 km/s is reached. As can be seen
in the figure, the computed subcritical reflection travel times do not
agree with the secondary arrivals between 70 km and 110 km.

Now, applying the reflectivity method to the model in Fig. VI.6.3, the
above gradient is sufficient to reproduce large amplitudes in the retro-
grade travel-time branch of the observations (Fig. VI.6.4). The theoretical
amplitudes near the critical distance are large in comparison with the
observed ones. However, further attempts to model these amplitudes in
the context of laterally homogeneous models were not considered due to
the mentioned travel time discrepancies.

Interpretation of the main line section assuming a laterally varying
structure

From the results of previous profiling experiments and seismological
studies in southern Norway (Fig. VI.6.1) crustal structure and Moho
depth are expected to vary especially around the endpoints of the CANOBE
profile. It is essential at this stage to deduce a model for the first
200 km of the profile for which P_MP observations are available in addition
to the Pg and Pn phases. Close examination of Fig. VI.6.5 reveals that
strong P_MP amplitudes are confined to two distinct distance intervals.
The first is around 115 km and is considered to be near the critical
distance where relatively large amplitudes are expected. The second is
around 185 km and is limited to a few seismograms. The latter extreme
P_MP-amplitudes can be attributed to focusing effects caused by waves
touching a caustic. While modelling these large amplitudes, however, the
relatively early P_MP subcritical arrivals (Fig. VI.6.3) must be accounted
for. These suggest a thinner crust as compared to the laterally homogeneous
model of the previous section although the travel-times of the P_n arrivals
from 150 km onwards must still be retained.

The calculations for the laterally varying models are performed using
Cassell's (1982) box method (based on zero-order ray theory) where physical
medium parameters are defined at 1 x 1 km grid points. A model is presented
in Fig. VI.6.6 which produces good agreement between the theoretical and

observed travel times. The main features in the model consist of a Moho with a depth of 26 to 28 km off-coast which increases to 33 km over a distance of 30 km beneath the coastline. The velocity gradient directly above the Moho is similar to that in Fig. VI.6.3 except that it does not follow the topography of the Moho from 80 km onwards but remains at a constant depth and gradually fades away after 200 km as shown in Fig. VI.6.8. In the coastal area the main discontinuity, associated with a velocity jump from 6.8 to 7.5 km/s, occurs at a depth of 26-28 km and is overlying a velocity gradient zone reaching a velocity of 8.1 km/s at 34 km. In this region the Moho should be regarded as a transition zone in which its depth is not clearly defined. Beyond 110 km the Moho materializes into a first order discontinuity with a P_n velocity of 8.1 km/s. The upper mantle velocity gradient is approximately 0.008 s^{-1}.

Synthetic seismograms were calculated for Model 1 (Fig. VI.6.7). Note that zero-order ray theory as used here is not exact near caustics or crictical points. Nevertheless, the amplitude distribution in the synthetic section qualitatively justifies the choice of the model. The amplitude distribution exhibits distinct peaks corresponding to the critical point of the $P_M P$ travel time branch and the caustic. The first theoretical amplitude maximum is located at 95 km whereas the observed maximum is found to be at approximately 115 km. This discrepancy is not surprising as zero-order ray theory does not include wave effects in the critical region beyond the critical point. A similar phenomenon applies to the amplitudes near the caustic, which are exaggerated by zero-order ray theory.

The P_n arrivals begin to undulate at distances greater than 270 km. The interpretation of structures in this distance range is ambiguous as we cannot determine whether the travel time perturbations are caused by Moho topography or by lateral crustal variations or a combination of both.

In Fig. VI.6.8 two possible structural configurations are presented which satisfy the P_n travel time data. The modelling was done with the criterion

of fitting computed travel time curves to the trend of the two apparent velocities in the P_n arrivals. These are a model with a varying Moho (Model 1) and one with a varying surface layer thickness (Model 2).

Significant constraints are imposed on the interpretation when attempting to account for the late arrivals which occur between 16 and 20 s in the last 150 km of the main line. These arrivals appear to be surface multiples corresponding to the P_g, P_MP and P_n phases of the first arrivals. When calculating multiple ray paths for Model 1, we find that the corresponding travel times fall approximately 1 second short of the observed arrivals. This indicates that the mean crustal velocity is too high as these waves travel only in the crust. The required delay is achieved for Model 2 in Fig. VI.6.8 by introducing a Moho depth of 30 km and a mean crustal velocity of 6.16 km/s.

In Fig. VI.6.9 synthetic seismograms are calculated for Model 2. The increasing P_n amplitudes with distance are in general agreement with those in the observations, although the theoretical ones are not continuous throughout all the records. This inconsistency is caused by unavoidable lateral velocity gradients in the laterally varying model. The multiple arrivals, however, have much smaller relative amplitudes than those in the observations. In a few cases, some of the theoretical records lack arrivals due to difficulties in finding rays to each receiver location.

Discussion and Conclusions

In this study we have demonstrated that the use of amplitude information as a supplement to travel time data is essential in delineating earth structure. The outstanding example here is the extremely strong amplitudes in the P_MP branch, confined to a relatively small distance interval around 180 km, which appears to be created by a strong velocity gradient in the lower crust. In this respect, the calculations of amplitudes for 2-D media proved very important as compared to the 1-D amplitude calculations by the reflectivity method.

The Moho is found to be 27 to 28 km deep beneath the first 80 km of the
profile before it dips downward over a distance of 30 km beneath the coast
and subsequently levels out at a depth of approximately 34 km. The inter-
pretation of the record section presented is only approximate for the
last 300 km of the main line. Two structural models were proposed for
this distance range. In order to keep the results presented here consistent
with Kongsberg seismograph station data (Bungum et al (1980) find a Moho
depth of 34 km at Kongsberg - see Fig. VI.6.1), preference should be given
to Model 1 in Fig. VI.6.8. In this model the Moho becomes slightly shallower
as it approaches the margin of the Oslo Graben from the southwest. After
a distance of 310 km along the profile it appears to sink to 36 km from
where it, over a distance of 180 km, rises to a depth of approximately
35 km beneath the NORSAR array. This Moho depth is in general agreement
with Berteussen's (1977) Moho depth values which are based on spectral
ratio analysis of long period P waves recorded at NORSAR.

On the other hand, Model 2 of Fig. VI.6.8 resulted from an attempt to cor-
relate the strong secondary arrivals in the last 100 km of the profile,
interpreted as multiple surface reflections of the P_g, P_MP and P_n phases.
The travel time delays in the crust, which are required for the correlation
of these multiple phases, infer a decrease in mean crustal velocity by as
much as 0.3 km/s and an elevation of the Moho by 5 km in comparison with
Model 1. Still, the synthetic section (Fig. VI.6.9) for Model 2 was not
particularly successful in matching the amplitudes of multiple phases,
and the possibility remains that the phases in question have not been
correctly identified. So, in order to conform with previous investigations,
we adopt Model 1 as representative for the main profile.

S. Mykkeltveit
E.S. Husebye
B. Cassell (Univ. of Cambridge, UK)
R. Kanestrøm (Univ. of Bergen)

References

Berteussen, K.-A., 1977: Moho depth determinations based on spectral ratio analysis of NORSAR long period P-waves. Phys. Earth Planet. Int., 15, 13-27.

Bungum, H., S.E. Pirhonen and E.S. Husebye, 1980: Crustal thicknesses in Fennoscandia. Geophys. J.R. astr. Soc., 53, 759-774.

Cassell, B.R., 1982: A method for calculating synthetic seismograms in laterally varying media. Geophys. J.R. astr. Soc., 69, 339-355.

Kanestrøm, R. and K. Haugland, 1971: Profile section 3-4, In: Deep Seismic Sounding in Northern Europe, A. Vogel (ed.), Swedish Natural Science Research Council, Stockholm, 76-91.

Kanestrøm, R. and S. Nedland, 1975: Crustal structure of southern Norway: A reinterpretation of the 1965 Seismic Experiment. Publication No. 117 in the Norwegian Geotraverse Project. In: Seismic Investigations of the Crust and Moho in Southern Norway, R. Kanestrøm (ed.), Univ. of Bergen, Seismological Observatory.

Mykkeltveit, S., 1980: A seismic profile in southern Norway. Pure and Appl. Geophys., 118, 1310-1325.

Sellevoll, M.A. and R.E. Warrick, 1971: A refraction study of the crustal structure of southern Norway.

Tryti, J. and M.A. Sellevoll, 1977: Seismic crustal study of the Oslo Rift. Pure and Appl. Geophys., 115, 1061-1085.

Weigel, W., J. Hjelme and M.A. Sellevoll, 1970: A refraction profile through the Skagerrak from northern Jutland to Southern Norway. Geodætisk Inst., Meddelelse No. 45, 1-28.
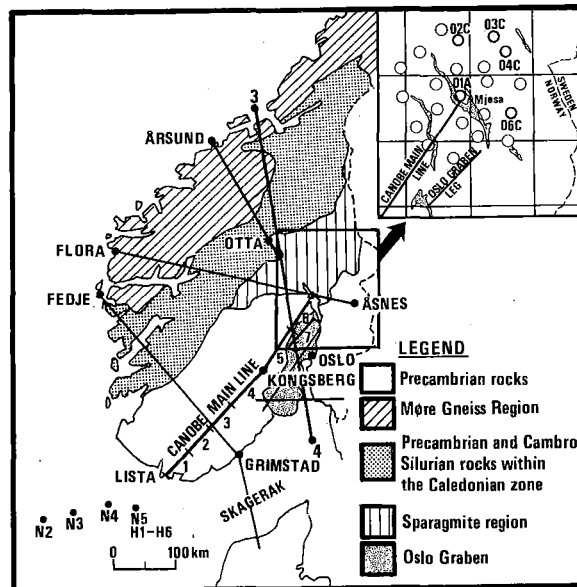
Fig. VI.6.1 Simplified geological map of southern Norway with CANOBE shot
points and recording legs. Results from previous profiles are
reported by Sellevoll & Warrick (1971) and Kanestrøm & Nedland
(1975) for the Flora-Åsnes and Fedje-Grimstad profiles, Kanestrøm
& Haugland (1971) for the '3-4'-profile, Tryti & Sellevoll
(1977) for profiles in the Oslo Graben, Weigel et al (1970) for
the Skagerrak profile and Mykkeltveit (1980) for the Årsund-
Otta profile. Also shown is the NORSAR array siting area with
the original 22 subarrays, each comprising 6 short period in-
struments. Five of the subarrays (bold rings) recorded the
CANOBE shots.
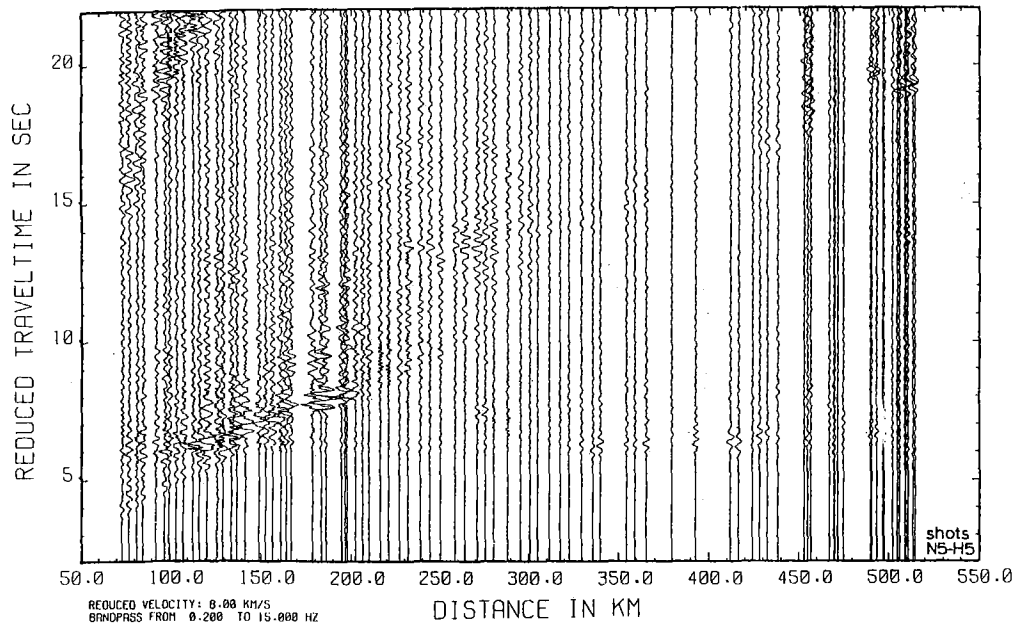
Fig. VI.6.2   Main line record section. Amplitudes are multiplied by distance
              and the seismograms are filtered between 0.2 and 15 Hz. The
              records beyond 450 km were recorded by the NORSAR array.
              The continuation of the crustal phase to the origin is not
              clear although an intercept time of 1.1 s indicates a travel
              time delay in the upper crust.
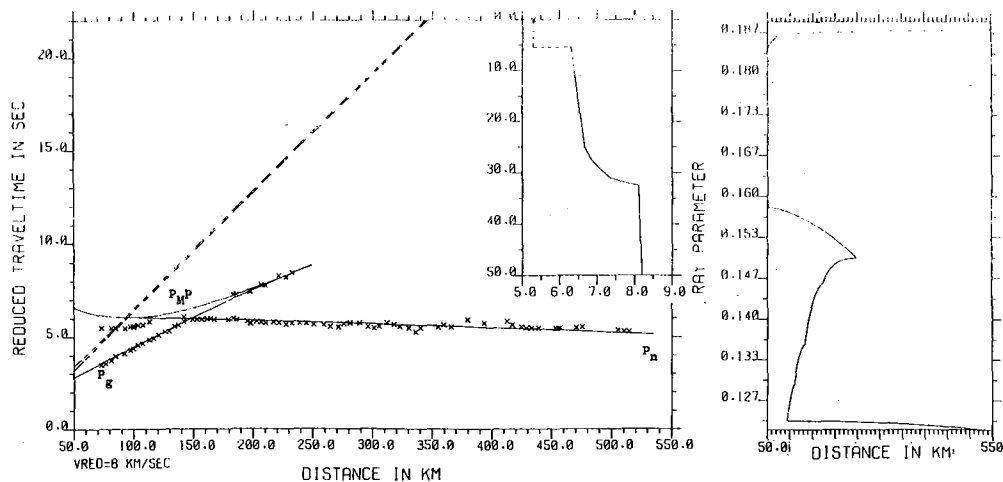
Fig. VI.6.3   Travel time-distance curves for the laterally homogeneous
              velocity-depth model (inserted). The portion of the velocity-
              depth function corresponding to unrecorded arrivals in the
              first 70 km of the record section is dashed. Crosses indicate
              observed arrivals. Note the discrepancy between observed and
              theoretical subcritical P_MP which indicates an elevated Moho
              beneath the first part of the profile.
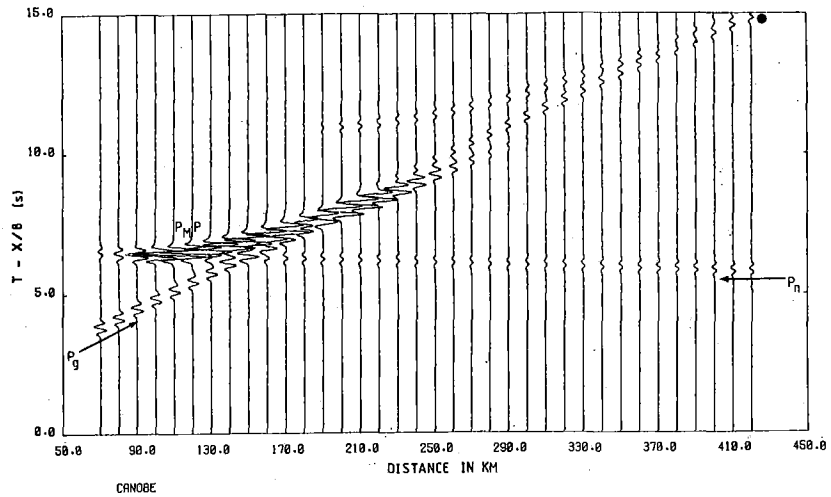
Fig. VI.6.4   Synthetic seismograms computed by the reflectivity method for
the model in Fig. VI.6.3. The source signal has a dominant
frequency of 3 Hz and 4 extrema. The dot indicates the outer
cusp in the P_MP-surface layer multiple caused by the artificial
first order discontinuity. The strong P_MP amplitudes are
produced by the velocity gradient in the crust. Amplitudes are
multiplied by distance.
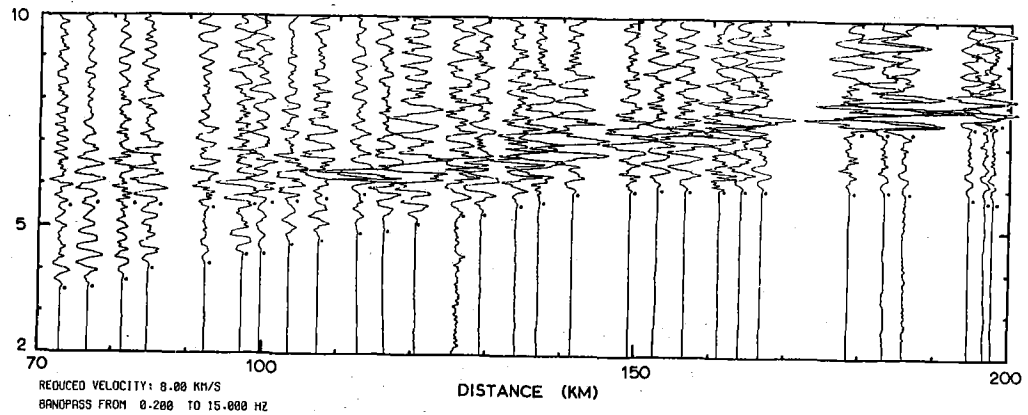
Fig. VI.6.5   Arrival picks in the main line record section. Amplitude maxima
in the secondary arrivals occur at 115 and 185 km.
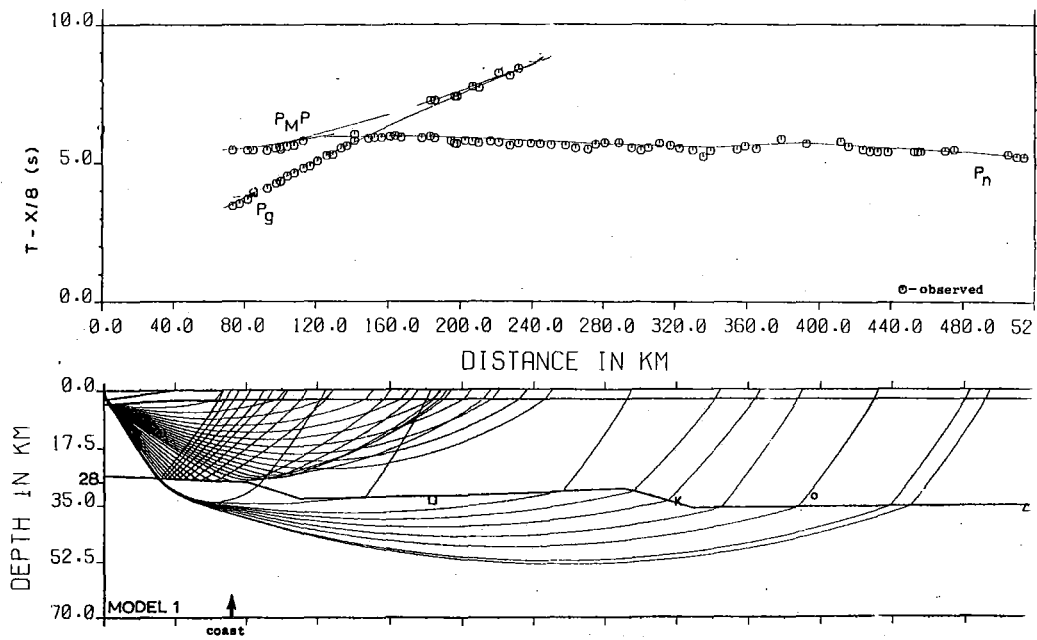
Fig. VI.6.6   Comparison of observed travel times and theoretical ones computed for Model 1 in Fig. VI.6.8. The vertical radii of the symbols indicating the observed times represent the reading errors. K denotes the Moho depth derived from Kongsberg seismograph station data. (Bungum et al, 1980)
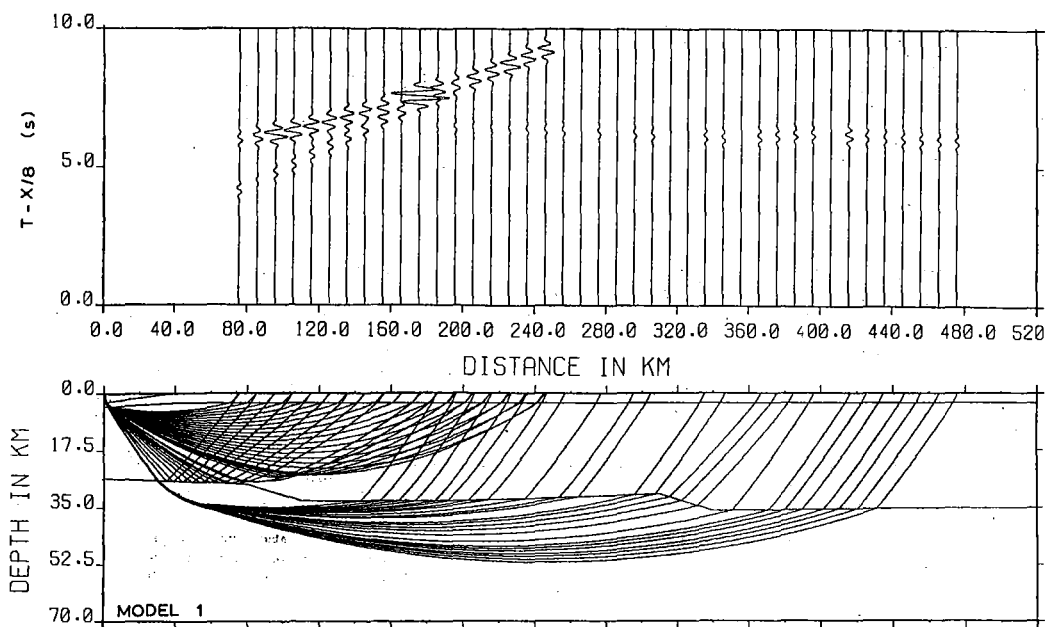
Fig. VI.6.7   Synthetic seismograms for the box method (Cassell, 1982). The source wavelet has a dominant frequency of 3.1 Hz, and amplitudes are multiplied by distance. Note the large amplitude at 176 km resulting from the velocity gradient in the lower crust.
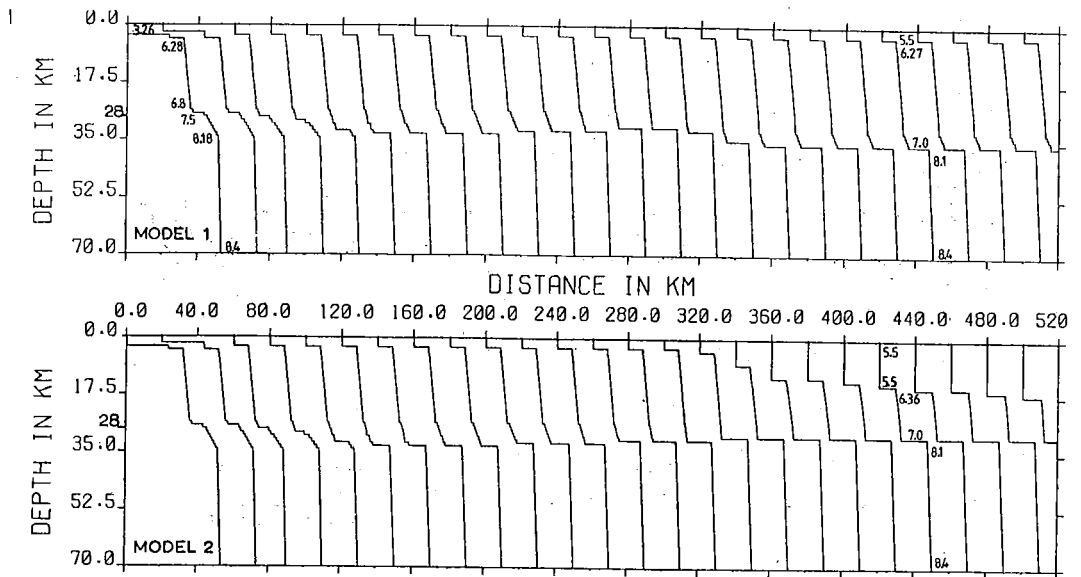
Fig. VI.6.8 Velocity-depth distributions for Models 1 and 2. The first order
discontinuity in the crust after 340 km for Model 2 has not
been observed and serves only to signify a decrease in the mean
crustal velocity in that area.
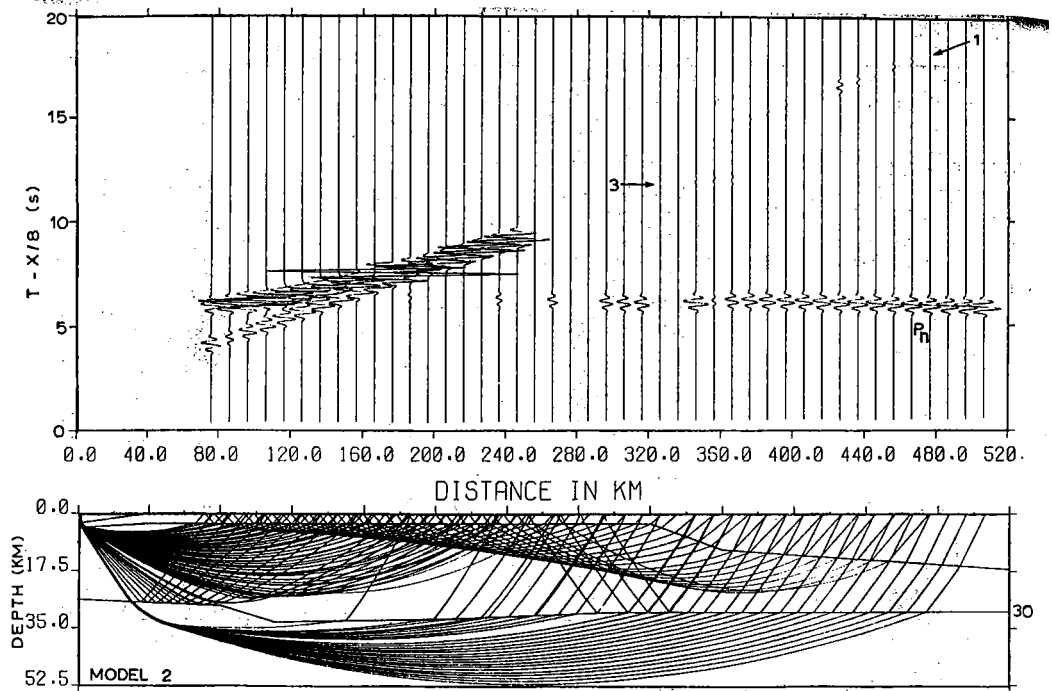
Fig. VI.6.9 Ray paths and synthetic seismograms for Model 2 in Fig. VI.6.8.
The multiple arrivals '1' and '3' have smaller amplitudes than
the corresponding observed phases.

VI.7   Fennoscandian noise survey

During the summer and fall of 1981, the first part of a noise study was performed involving various sites in Finland, in northern Norway (Finmark), and in southeastern Norway. The purpose of this survey, which still continues, is to measure the ambient noise level as a function of frequency for various sites in Fennoscandia, and to measure noise correlation as a function of short interstation distances for some of these sites. Special emphasis has been given to high frequencies, in order to obtain information relevant to the construction and possible deployment of small aperture seismic arrays aimed at detection and analysis of regional seismic signals.

Recording equipment and logistics

The main field equipment used has been Kinemetrics PDR-2 'Compuseis' recorders combined with Geotech S-13 seismometers, and preamplifiers were needed in order to obtain sufficient amplitude resolution for the background noise. The data were recorded on cassettes and subsequently played back using a Kinemetrics CCS-1 playback system and an IBM 4341 computer. A nuch faster playback procedure was later developed based on a PDP 11/34 computer, and the development of these programs was an effort that was completed late spring 1982.

In addition to the data recorded by the PDR-2 field recorders, the noise study has also included some 40 Hz NORESS data recorded at the NORSAR data center. These data, from 8 of the NORESS seismometers, have been transmitted in analog form to Kjeller and recorded there via the new MODCOMP/IBM 4331 connection.

Methods of analysis

The procedure for computing power spectra depends on the nature of the data under analysis. Basically, these would fall into three main categories:

a)   Transient signals:

The Energy Density is estimated as

$$P_x(f) = \Delta t^2 X(f)\overline{X(f)} \qquad (nm^2/Hz^2)$$

where
$$X(f) = \sum_{n=0}^{N-1} x(n)\exp(-2\pi i f n/N)$$

$$\Delta t = \text{sampling interval (sec)}$$
$$N = \text{number of samples}$$

b) Stationary signals (noise):

The Power Density is estimated as

$$P_x(f) = \frac{\Delta t}{N} X(f)\overline{X(f)} \qquad (nm^2/Hz)$$

or with block averaging (M blocks)

$$P_x(f) = \frac{\Delta t}{N \cdot M} \sum_{j=1}^{M} X_j(f)\overline{X_j(f)}$$

c) Periodic signals:

The Power is estimated as

$$P_x(f) = \frac{1}{N^2} X(f)\overline{X(f)} \qquad (nm^2)$$

It is the definition under b) which has been used in the present case, for analysis of stationary noise, while a) would be required for analysis of earthquake or explosion signals. Needless to say, the normalization procedure is important when faced with the problem of computing spectra with reference to absolute ground motion.

Noise correlation ρ (zero lag only) has been computed using the same block lengths as for the spectral estimates and averaged over the same number of blocks. The estimates are considered only as functions of interstation distances

(azimuth not used), and averages have been computed over certain distance intervals. Since correlations are bounded by unity, they are not normally distributed and standard deviations can therefore not be computed the conventional way. This problem was solved by transforming the correlations into a new variable:

$$z = \tfrac{1}{2} \left[\ell n(1+\rho) - \ell n(1-\rho) \right]$$

which will be almost normally distributed as shown by Fisher. Confidence limits are then taken as $z = \bar{z} + \sigma_z$ and $z = \bar{z} - \sigma_z$, and the corresponding levels in ρ are found by the transformation:

$$\rho = \tanh(z)$$

Results

The sites which have been analyzed so far are shown in Fig. VI.7.1 and their names and locations are listed in Table VI.7.1, where also the main results in terms of spectral levels are given. For most of the locations at least 2 time intervals are presented, with results given for 7 frequencies, each separated by one octave.

It should be noted here that for all of the locations from 1 to 7, where the PDR-2 field equipment was used, there was a considerable problem in finding time intervals that were not contaminated by high frequency noise of more transient nature. The sources here were mostly of cultural origin, but also in some cases wind and effects due to poor coupling between seismometer and ground (for many of the sites the seismometers were placed on surface exposure of rock). This problem is of course connected to the fact that we are interested in very low levels of the the ambient noise (down to 0.01 nm) and at frequencies much higher than with more conventional seismometers (sampling rate 62.5 Hz, high-cut filter at 25 Hz). For the future measurements we will counter this problem by more careful siting, concrete pads for the seismometers, wind protection, etc.

In addition to the first sites listed in Table VI.7.1, where the PDR-2 equipment was used, we have also analyzed some intervals of 40 Hz NORESS data as mentioned above. The reason why the results there are given only up to 4 Hz is that the linearly ranged quantum unit for that temporary system is too large to give sufficient amplitude resolution for higher frequencies.

Among the conclusions that can be drawn from the spectral results are the following:

1) The spectral level at 1 Hz is for most sites in the range between 0 and 10 dB relative to 1 nm^2/Hz. Although this is 10-20 dB higher than the SRO/ASRO low noise points (Peterson, 1980) and the Queen Creek level (Fix, 1972), it is still a reasonably good level as compared to most seismic stations of the world.

2) The slope of the spectrum falls off with about 20 dB/octave from 0.25 Hz and up to 1.5-2.0 Hz; above that frequency the slope is around 10 dB/octave all the way up to 16 Hz (see also Fig. VI.7.2). This is contrary to the stronger reduction in slope which is commonly observed for frequencies above about 5 Hz. We have confidence in our results here, however, since i) our use of preamplifier asures a good quantification for the noise, and ii) the high cut-off filter and sampling frequency gives a good relative response at these higher frequencies (see Fig. VI.7.3).

3) The noise level at 0.25 Hz (which is the location of the well-known microseismic peak) shows much stronger variation in time than in space. It is clear that the noise level up to at least 1 Hz correlates (although with much smaller fluctuations) with these 4-second microseisms, which are mostly attributed to atmospheric disturbances over oceans. This is consistent with the change in spectral slope around 2 Hz which could indicate two separate noise processes (Adair, 1982), and it is also consistent with the results of Ringdal and Bungum (1977) who studied long-term noise variation within different frequency bands at NORSAR.

4) Although there is a tendency (as expected) that the Finnish sites get quieter as one moves eastward, the noise levels there are not significantly better than those observed in southeastern Norway. The northern Norway sites, on the other hand, seem to be slightly higher in noise level, which should be expected from the proximity of these sites to the offshore noise-generating areas.

5) For most of the noise data analyzed so far, there is no significant difference between vertical and horizontal components. In a few cases, however, the horizontal components show a slightly higher noise level.

Results in terms of noise correlation are presented in Figs. VI.7.4-6, where Fig. VI.7.4 is from location 7, covering distances from 50 to 600 m. The scatter in the results is fairly large, which in part is due to the fact that the data are taken from non-simultaneous measurements (3 seismometers were successively moved around to 12 sites), and in part caused by the previously mentioned high-frequency transient noise disturbances. There are clear indications in Fig. VI.7.4 that negative correlation occurs at certain distances (dependent on frequency bands), which was shown by Mykkeltveit et al (1982) to be consistent with a model of propagating noise under isotropic conditions.

Correlation results from the NORESS array sampled at 40 Hz are shown in Figs. VI.7.5-6, where the confidence limits now are much smaller. The tendency for the noise to correlate negatively is now even clearer, although the negative deflection is not as pronounced as in the 20 Hz NORESS results presented by Mykkeltveit et al (1982).

The examples in Figs. VI.7.5-6 are picked out so as to show a large difference in correlation levels in the first frequency band (1-3 Hz). It is interesting to note that although there may be a small difference also in the 2-3 Hz band, there is no difference for higher frequencies. It seems therefore that the main correlation variations tend to occur within the frequency band covered by the steepest part of the spectrum (up to 1.5-2.0 Hz), which again point towards different noise processes below and above this frequency.

There is another interesting observation in the fact that the data used in
Fig. VI.7.5 (day 80/1982) and in Fig. VI.7.6 (day 130/1982) have reasonably
similar spectra (see Table VI.7.1), in spite of very different correlation
levels. There is, however, a difference in the sense that the spectrum for
day 80 (Fig. VI.7.5) peaks at a higher frequency than for day 130 (Fig.
VI.7.6). This points towards a smaller distance to the main noise generation
area and possibly shallower water if ocean-generated (cf. Bungum et al,
1971). In fact, the 1-3 Hz noise correlation on day 80 is higher than for
any of the other NORESS intervals included in Table VI.7.1, which all
fall between the levels of days 80 and 130. It should be mentioned here that
some correlation measurements obtained at location 4 are consistent with
the results presented above.

The main conclusion in terms of noise correlation is therefore that there
is a fairly good stability in time and space for frequencies above about 2 Hz,
while there is some variation in time for lower frequencies. This variation
correlates more with the shape of the noise spectrum than with the absolute
level, pointing towards differences in the noise-generating areas as the
main factor of influence with respect to the correlation properties of the
noise.

H. Bungum

References

Adair, R., J. Orcutt and T.H. Jordan, 1982: The Marine Seismic System: signals
and noise. DARPA Symposium on seismic detection, analysis, discrimination
and yield estimation. Hampton, Va., 25-27 May 1982.

Bungum, H., E. Rygg and L. Bruland, 1971: Short-period seismic noise structure
at the Norwegian Seismic Array. Bull. Seism. Soc. Am., 61, 357-373.

Fix, J.E., 1972: Ambient earth motion in the period range from 0.1 to 2560 sec.
Bull. Seism. Soc. Am., 62, 1753-1760.

Mykkeltveit, S., K. Åstebøl, D.J. Doornbos and E.S. Husebye, 1982: Seismic
array configuration optimization. Submitted to Bull. Seism. Soc. Am.

Peterson, J., 1980: Preliminary observations of noise spectra at the SRO and
ASRO stations. USGS Open File Report 80-992, Albuquerque, New Mexico.

Ringdal, F. and H. Bungum, 1977: Noise level variation at NORSAR and its
effect on detectability. Bull. Seism. Soc. Am., 67, 479-492.

NORSAR NOISE STUDY SITES
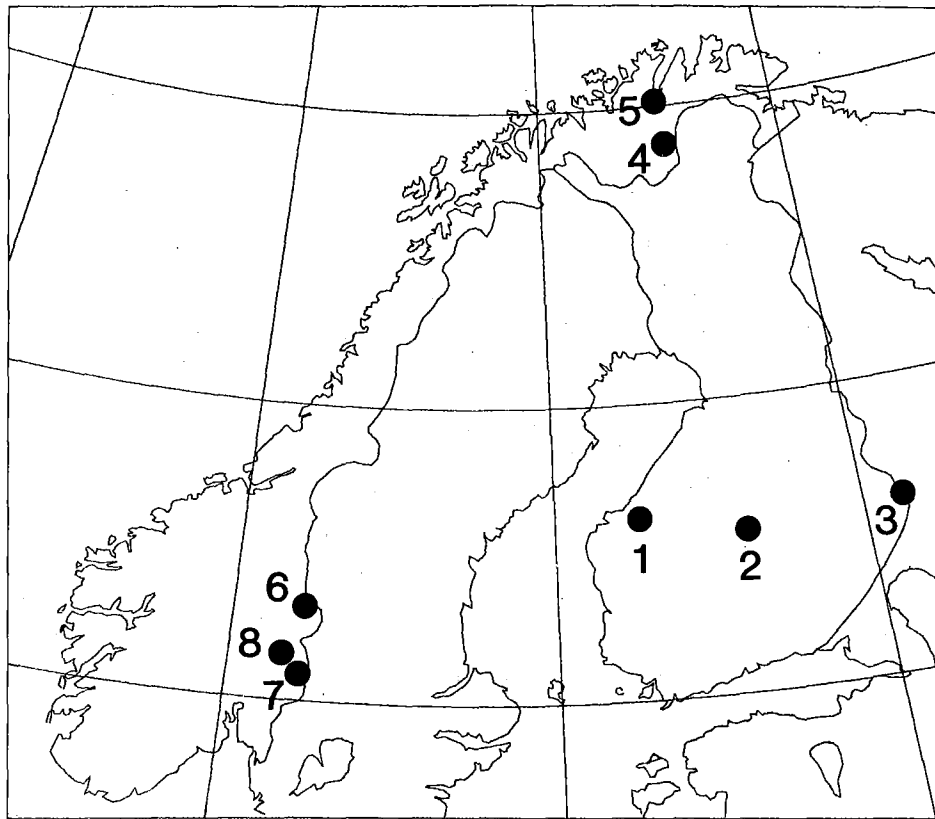
Fig. VI.7.1 Sites for the Fennoscandian noise survey 1981/82.

LOCATION		LAT.	LONG.	1981		POWER	DENSITY	(DB	REL	TO	1	NM**2)
NO	NAME	(°N)	(°E)	DAY	HOUR	.25	.50	1.0	2.0	4.0	8.0	16.
1	HOOPAKKA	63.05	22.71	250	1733	54	33	12	-13	-25	-38	-53
					2000	53	33	10	-15	-28	-40	-52
2	SUMIAINEN	62.72	26.15	251	1648	52	28	7	-15	-28	-40	-47
					2304	48	28	2	-16	-31	-42	-53
3	ILOMANTSI	62.92	31.31	254	1701	47	23	-2	-18	-28	-40	-52
				255	0932	45	20	-1	-21	-29	-40	-52
4	KARASJOK	69.35	25.17	223	1815	53	31	5	-12	-26	-39	-48
					2014	54	31	6	-13	-27	-40	-50
5	LAKSELV	70.03	25.00	224	1324	55	29	6	-12	-21	-32	-45
					1329	55	30	7	-12	-25	-36	-43
6	ENGEREN	61.55	12.19	232	2000	48	25	-1	-17	-33	-43	-53
					2202	48	27	2	-15	-30	-42	-53
7	KIRKENAER	60.41	12.14	301	1403	53	33	8	-9	-20	-32	-46
				1982								
8	NORESS	60.74	11.54	80	1000	39	27	4	-17	-28		
				84	1510	50	30	8	-13	-27		
				123	1350	52	30	3	-17	-30		
				130	1355	37	23	2	-16	-27		
				189	2105	42	26	0	-17	-28		

Table VI.7.1 Name and location for the 8 noise survey sites shown in Fig. VI.7.1.
The power spectral level for each of the sites are given for 7
frequencies, each separated by one decade.
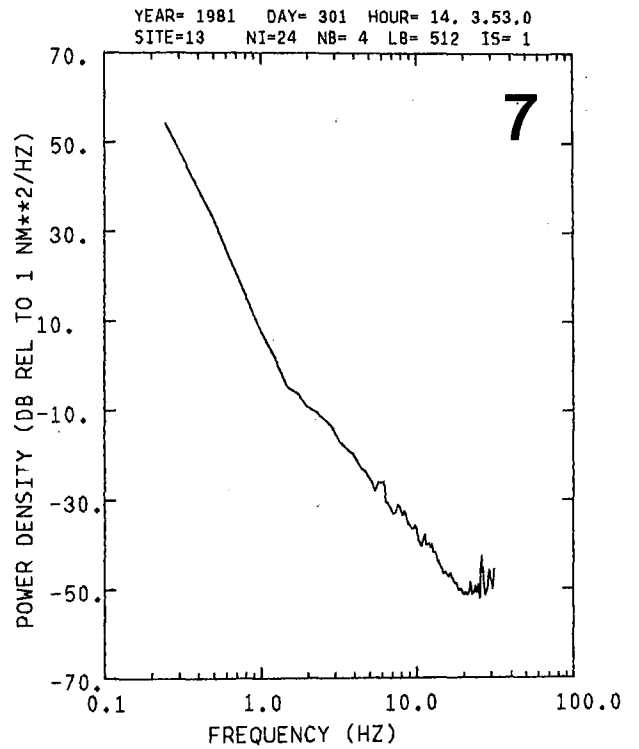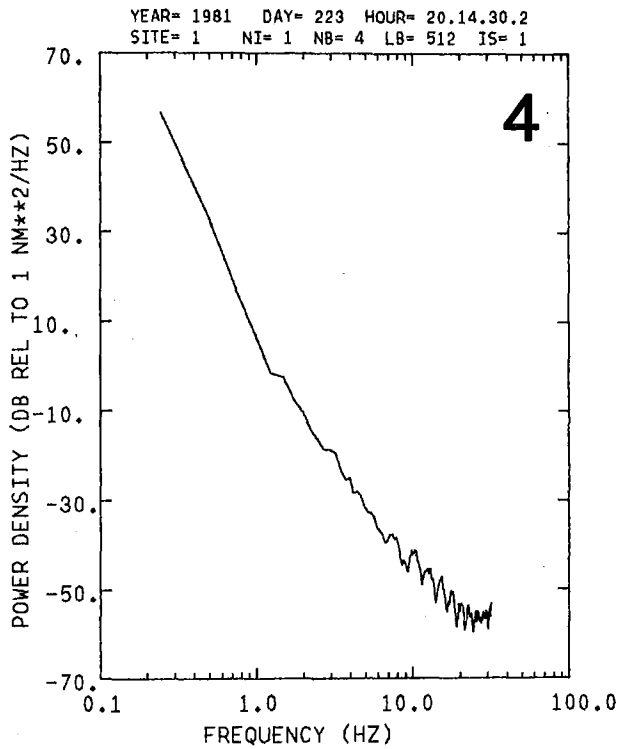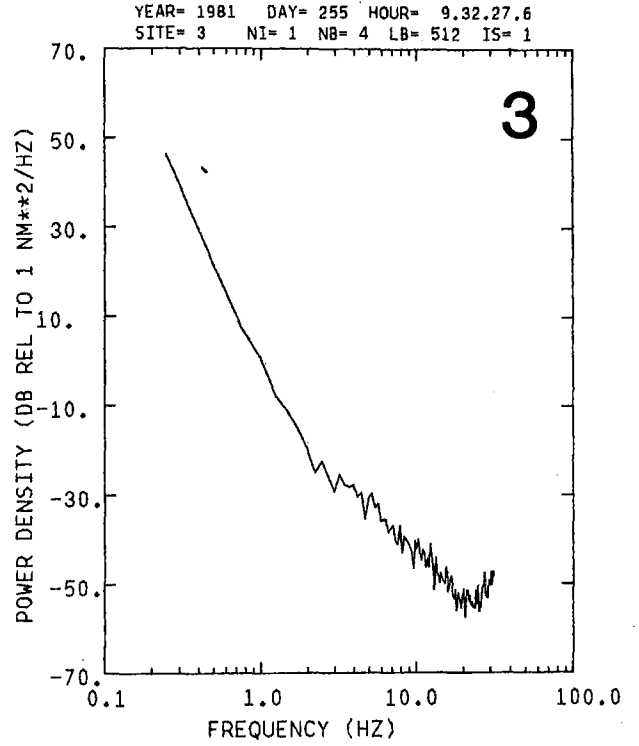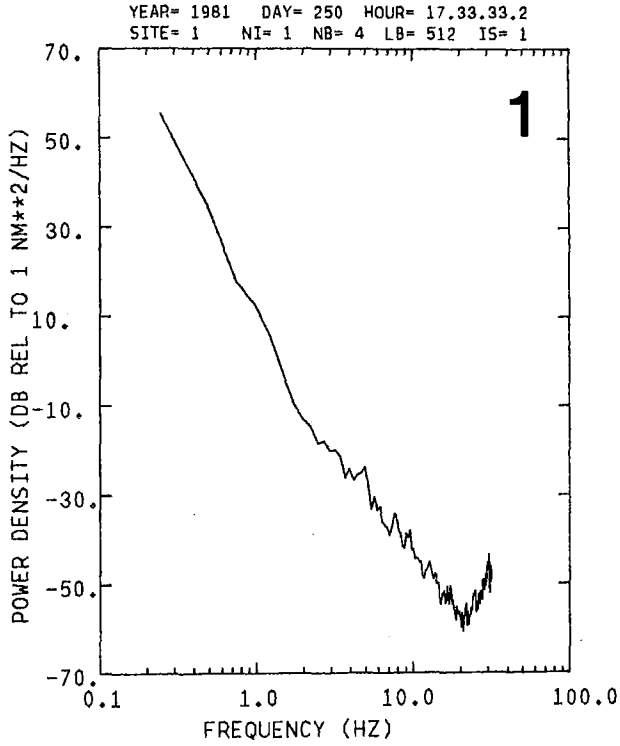
Fig. VI.7.2   Noise spectra from locations no. 1, 3, 4 and 7. The first 3 are from single seismometers, while no. 7 is averaged over 12 sites within 600 m of each other. Each spectrum is averaged over 4 blocks of data, each 512 samples long, and the sampling frequency is 62.5 Hz with an anti-aliasing filter at 25 Hz.
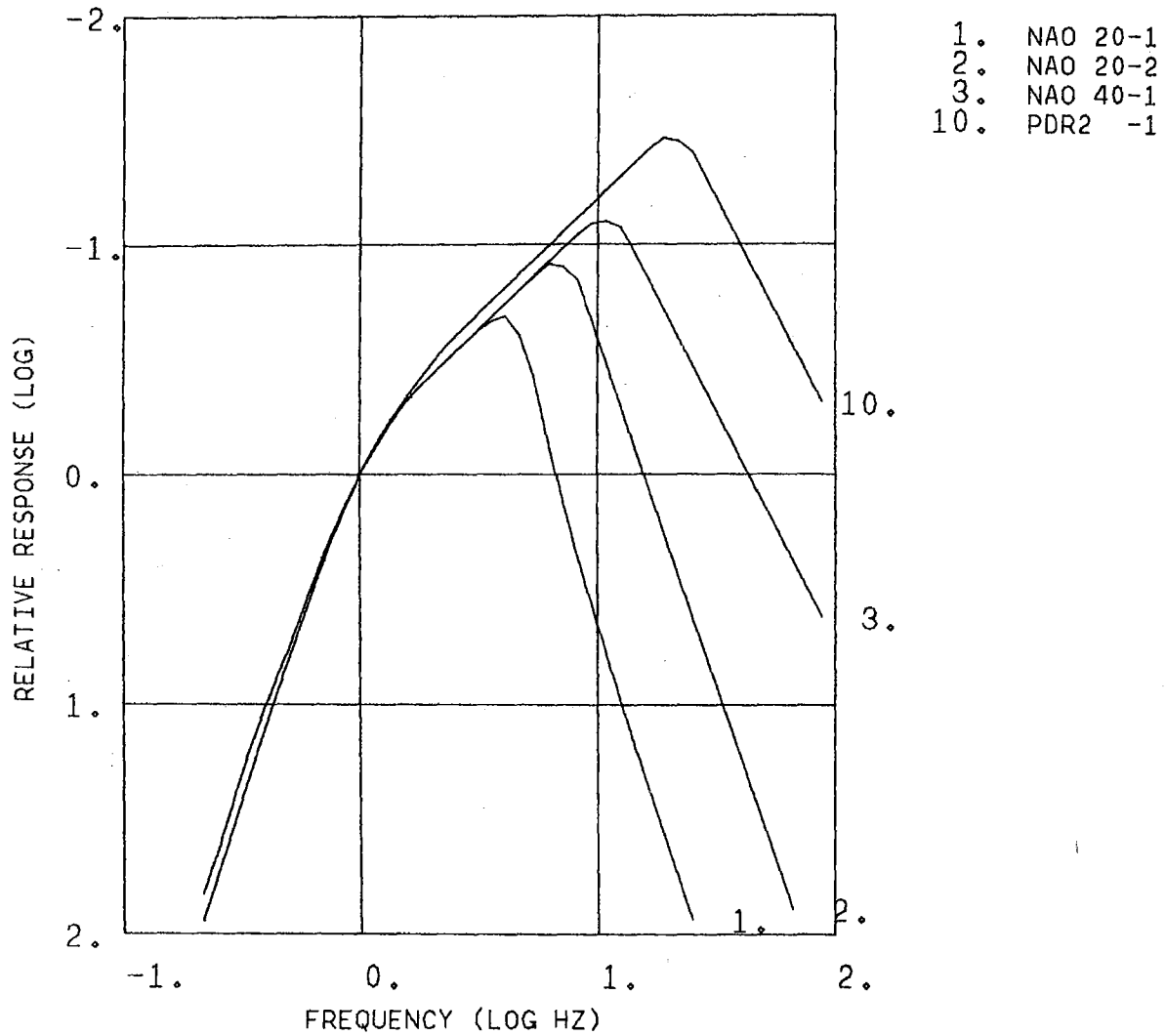
Fig. VI.7.3   Relative response functions for

1.   NORSAR, 20 Hz sampling, 5 Hz filter
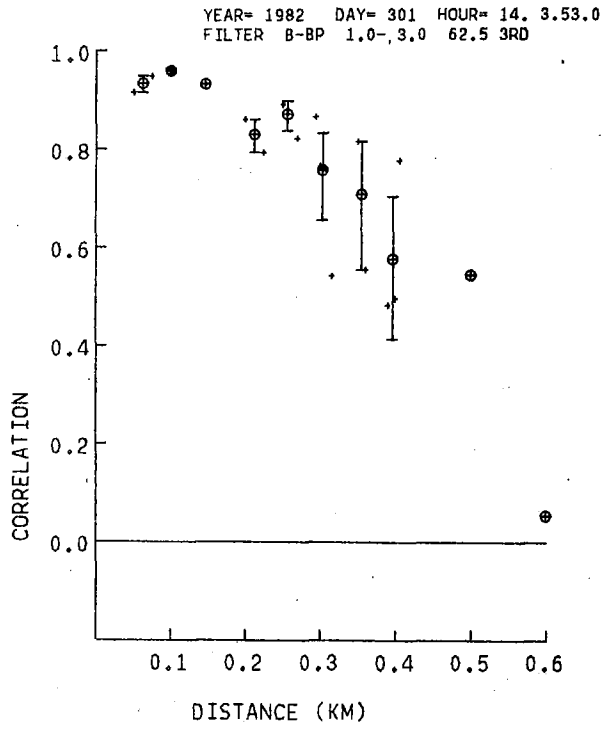2.   NORSAR, 20 Hz sampling, 8 Hz filter
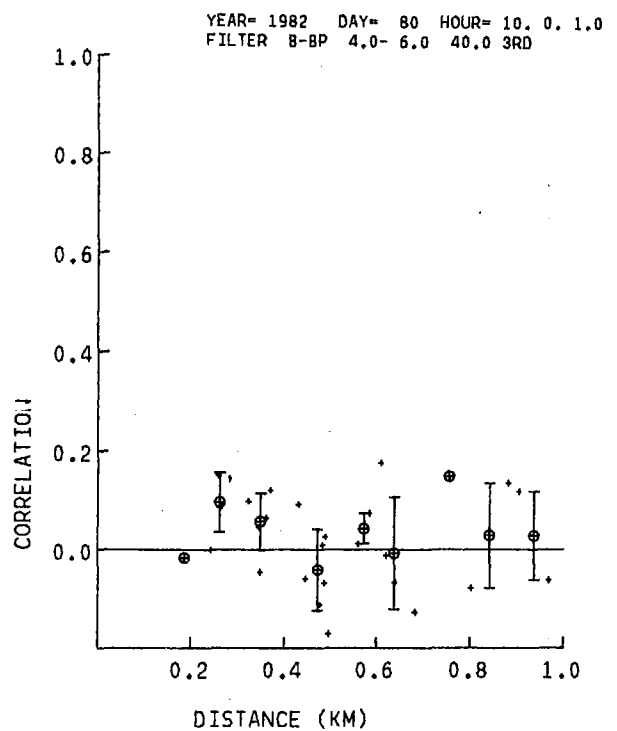3.   NORSAR, 40 Hz sampling, 12.5 Hz filter
4.   PDR-2, 62.5 Hz sampling, 25 Hz filter
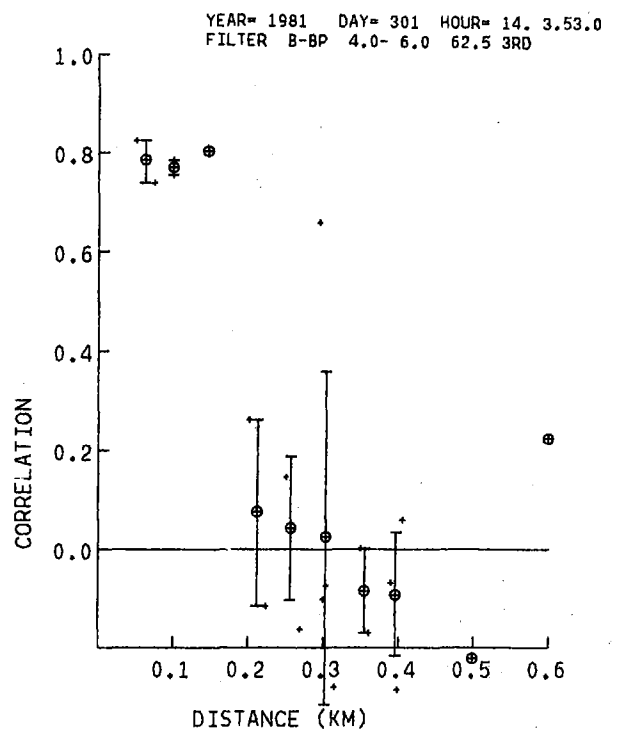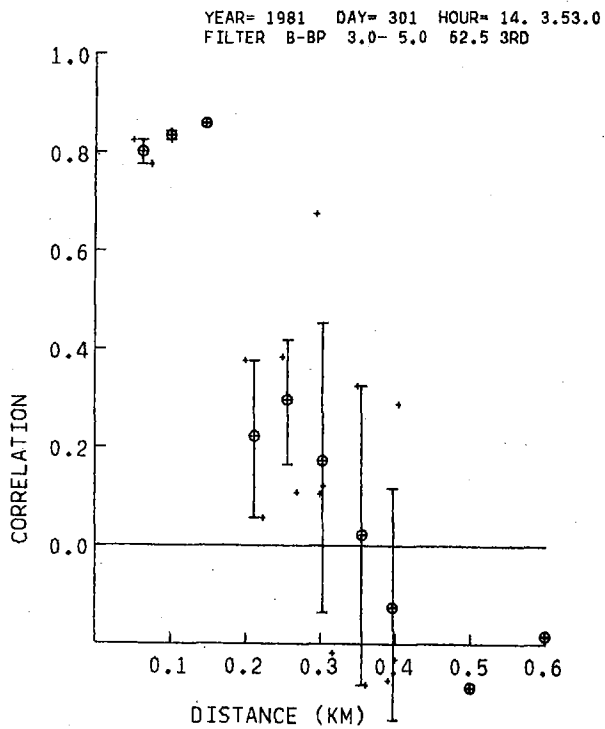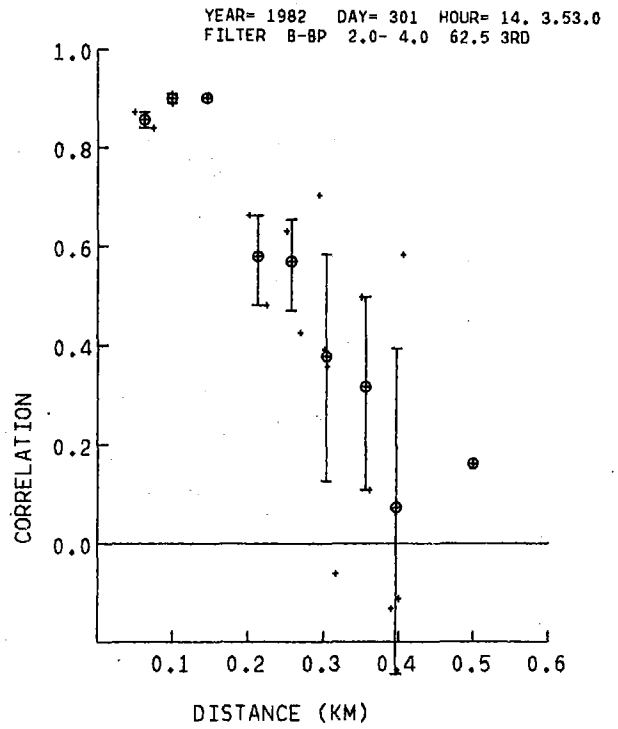
Fig. VI.7.4 Noise correlation vs. distance for location no. 7 (see Table VI.7.1), where 3 seismometers were successively moved around to cover inter-station distances between 50 and 600 m. The four graphs cover the frequency bands 1-3, 2-4, 3-5 and 4-6 Hz, respectively.

YEAR= 1982   DAY= 130   HOUR= 13.55. 0.5
FILTER B-BP 1.0- 3.0   40.0 3RD

YEAR= 1982   DAY= 130   HOUR= 13.55. 0.5
FILTER B-BP 2.0- 4.0   40.0 3RD

YEAR= 1982   DAY= 130   HOUR= 13.55. 0.5
FILTER B-BP 3.0- 5.0   40.0 3RD

YEAR= 1982   DAY= 130   HOUR= 13.55. 0.5
FILTER B-BP 4.0- 6.0   40.0 3RD
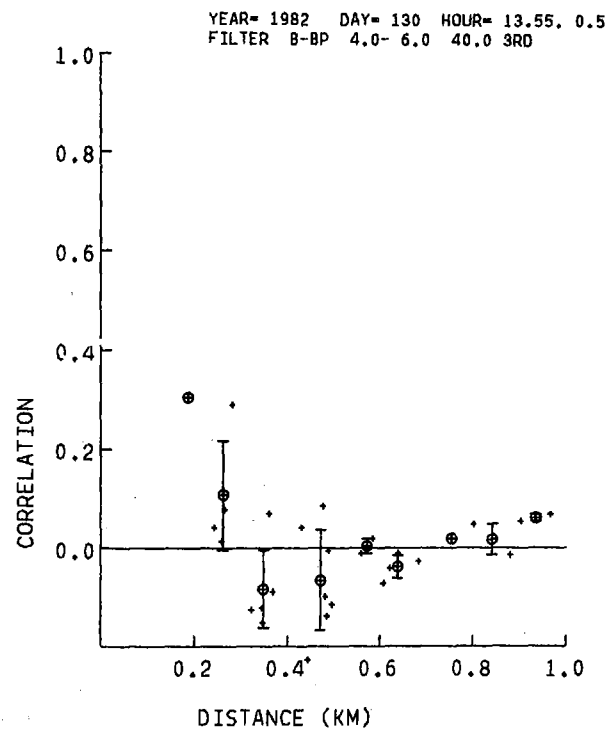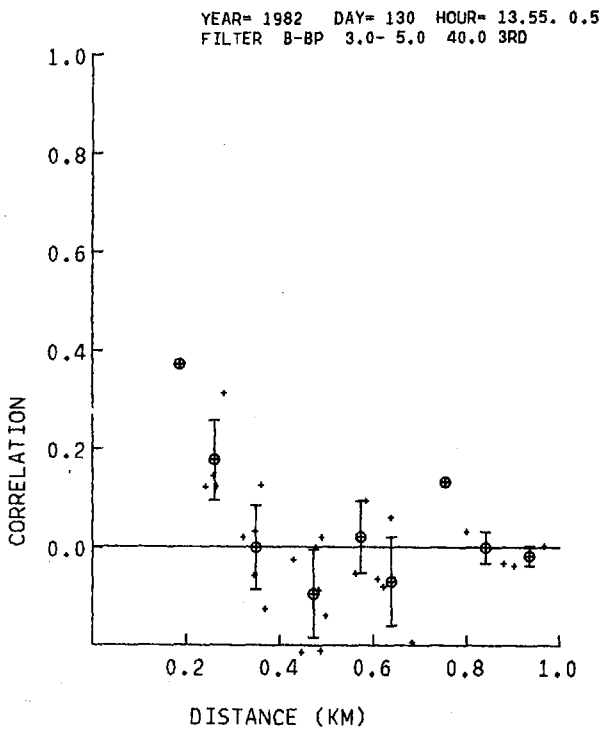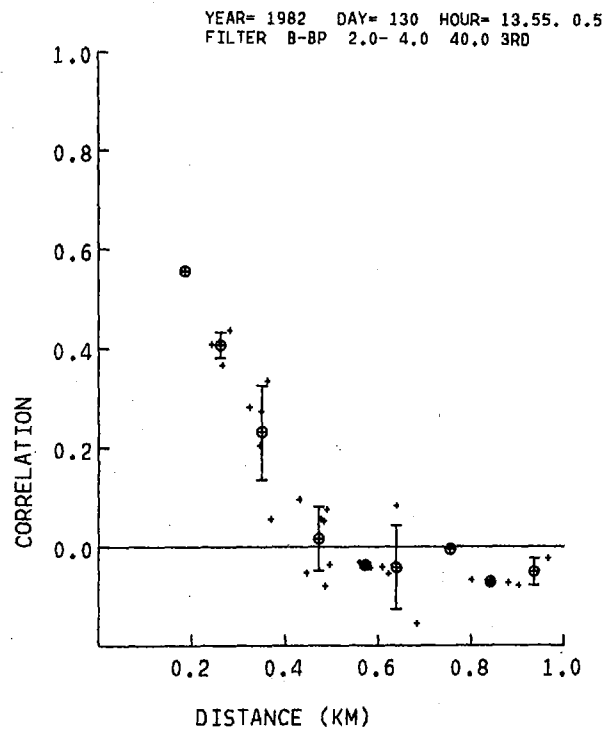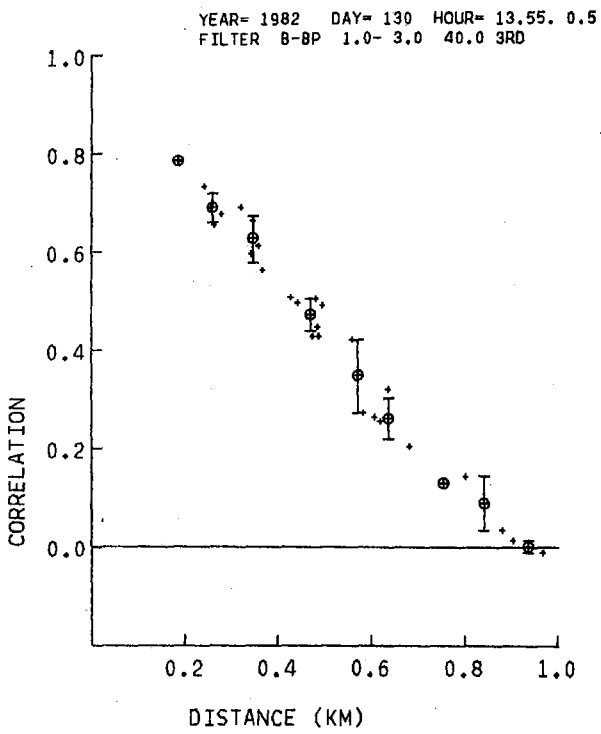
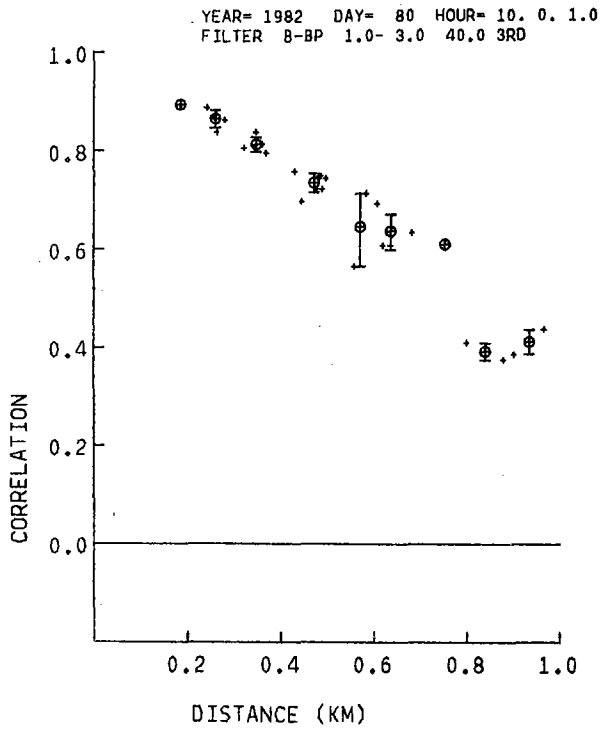Fig. VI.7.6   Same as for Fig. VI.7.5, but for day 130/1982.
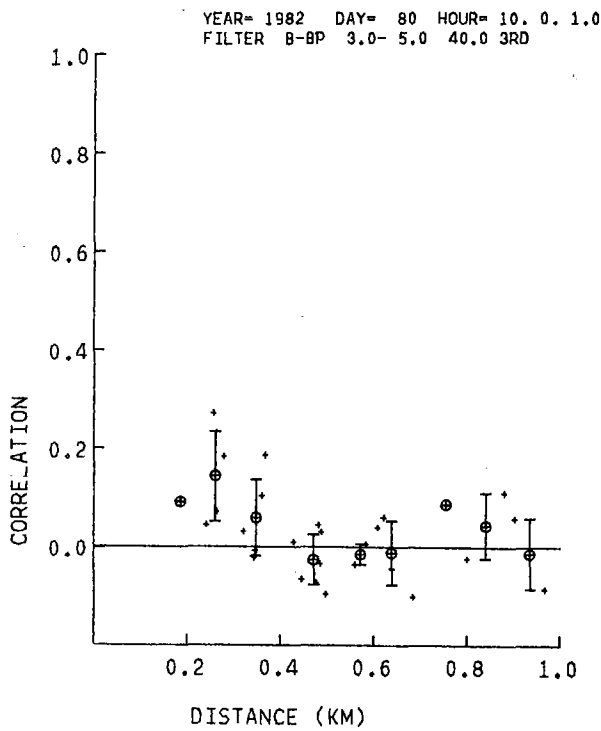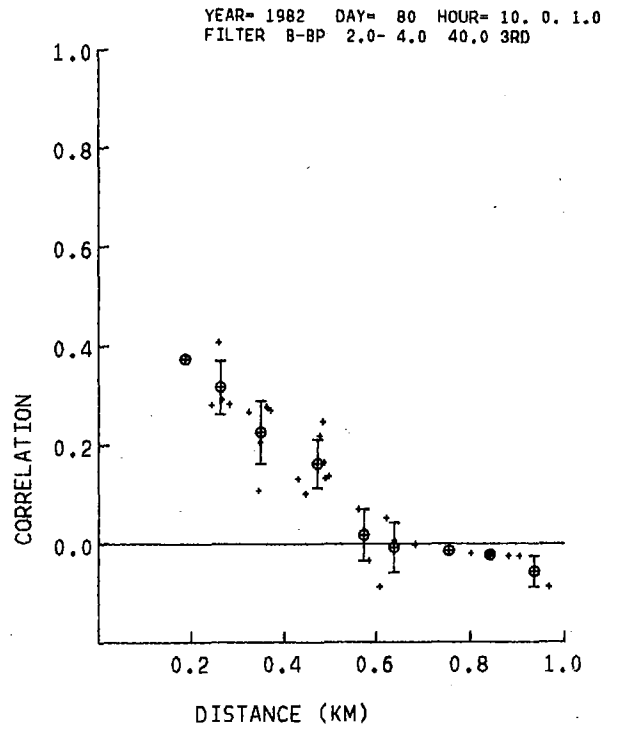
Fig. VI.7.5 Noise correlation vs. distance for location no. 8 (NORESS) and
day 80/1982 (see Table VI.7.1). Eight channels sampled at 40 Hz
have been used, and the frequency bands for the four graphs
are the same as for Fig. VI.7.4.